Spectroscopy of Free-Base N-Confused Tetraphenylporphyrin Radical Anion and Radical Cation

ARTICLE *in* THE JOURNAL OF PHYSICAL CHEMISTRY A · JUNE 2011

Impact Factor: 2.69 · DOI: 10.1021/jp200411q · Source: PubMed

THE JOURNAL OF PHYSICAL CHEMISTRY A

ARTICLE

pubs.acs.org/JPCA

Spectroscopy of Free-Base N-Confused Tetraphenylporphyrin Radical Anion and Radical Cation

Elvin A. Alemán,[†] Juan Manríquez Rocha,[‡] Wongwit Wongwitwichote,[†] Luis Arturo Godínez Mora-Tovar,[*,‡] and David A. Modarelli[*,†]

[†]Department of Chemistry and The Center for Laser and Optical Spectroscopy, Knight Chemical Laboratory, The University of Akron, Akron, Ohio 44325-3601, United States

[‡]Centro de Investigación y Desarrollo Tecnológico en Electroquímica S.C., Parque Tecnológico Querétaro Sanfandila, C.P. 76703, Pedro Escobedo, Querétaro, México

Supporting Information

ABSTRACT: The radical anions and radical cations of the two tautomers (**1e** and **1i**) of 5,10,15,20-tetraphenyl N-confused free-base porphyrin have been studied using a combination of cyclic voltammetry, steady state absorption spectroscopy, and computational chemistry. N-Confused porphyrins (NCPs), alternatively called 2-aza-21-carba-5,10,15,20-tetraphenylporphyrins or inverted porphyrins, are of great interest for their potential as building blocks in assemblies designed for artificial photosynthesis, and understanding the absorption spectra of the corresponding radical ions is paramount to future studies in multicomponent arrays where electron-transfer reactions are involved. NCP **1e** was shown to oxidize at a potential of E_{ox} 0.65 V vs $Fc^+|Fc$ in DMF and reduce at E_{red} −1.42 V, while the corresponding values for **1i** in toluene were E_{ox} 0.60 V and E_{red} −1.64 V. The geometries of these radical ions were computed at the B3LYP/6-31+G(d)//B3LYP/6-31G(d) level in the gas phase and in solution using the polarizable continuum model (PCM). From these structures and that of H_2TPP and its corresponding radical ions, the computed redox potentials for **1e** and **1i** were calculated using the Born−Haber cycle. While the computed reduction potentials and electron affinities were in excellent agreement with the experimental reduction potentials, the calculated oxidation potentials displayed a somewhat less ideal relationship with experiment. The absorption spectra of the four radical ions were also measured experimentally, with radical cations $\mathbf{1e}^{\bullet+}$ and $\mathbf{1i}^{\bullet+}$ displaying significant changes in the Soret and Q-band regions as well as new low energy absorption bands in the near-IR region. The changes in the absorption spectra of radical anions $\mathbf{1e}^{\bullet-}$ and $\mathbf{1i}^{\bullet-}$ were not as dramatic, with the changes occurring only in the Soret and Q-band regions. These results were favorably modeled using time-dependent density functional calculations at the TD-B3LYP/6-31+G(d)//B3LYP/6-31G(d) level. These results were also compared to the existing data of free base tetraphenylporphyrin and free base tetraphenylchlorin.

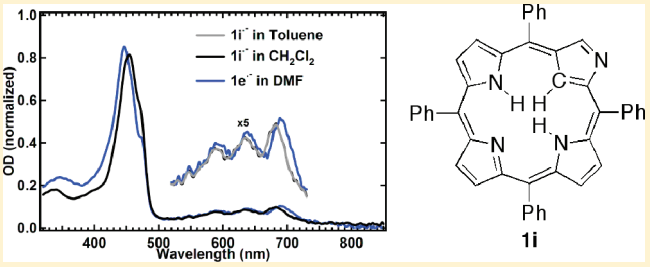

I. INTRODUCTION

The photophysical properties of porphyrins have been studied for many years and are reasonably well understood.[1,2] Research in this area, however, continues to further the understanding of the dynamic events occurring upon light absorption in the light-harvesting complexes (LHCs) and photosynthetic reaction centers (PRCs) in purple bacteria and green plants.[3−5] In these systems, the various BChl*a*[6,7] groups in the light-harvesting centers of green plants (LHCII)[3] and purple bacteria (LH2[4] and LH1)[5] transfer energy efficiently into the photosynthetic reaction center (PRC), exciting the so-called "special pair" of bacteriochlorophylls $(BChl\,a)_2$. The electronically excited special pair in turn initiates a series of rapid photoinduced electron transfers (ET) to a quinone electron acceptor. The resulting oxidized $(BChl\,a)_2$ is reduced to its neutral state through the oxidation of water, while the reduced quinone is transported outside the PRC membrane where it provides an electron for the various processes involved in cellular energy production.[6] Efforts to replicate these processes using synthetic assemblies have resulted from increasing interest in solar energy conversion schemes.

The syntheses of derivatives of bacteriochlorophyll are non-trivial,[8,9] and schemes for solar energy conversion designed to mimic the events in the LHCs and/or PRC have as a result often used arrays of free-base and metalloporphyrins as energy and electron donors.[10−14] However, the photophysical properties[8,9] of bacteriochlorophylls and the closely related chlorins are substantially different from those of regular porphyrins. The high symmetry of free-base (D_{2h}) and metallo (D_{4h}) porphyrins results in a near-degeneracy in the highest two occupied and lowest two unoccupied molecular orbitals (MOs), resulting in weak absorption features in

Received: January 14, 2011
Revised: May 12, 2011
Published: May 16, 2011

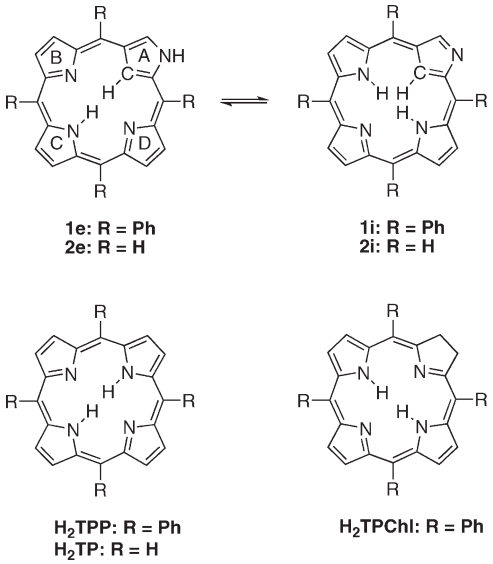

Figure 1. The tautomeric forms of N-confused tetraphenylporphyrins (**1e** and **1i**) and N-confused porphines (**2e** and **2i**). A, B, C, and D denote the nomenclature of the rings in top left structure.

the low energy region of the visible spectrum. In contrast, the degeneracy of these MOs is broken in the lower symmetry BChl*a*s (and related molecules), and as a result these molecules have significantly more intense low energy absorption bands that are substantially better optimized for the absorption of solar radiation. To more efficiently absorb energy in the solar spectrum, readily synthesized analogues of BChl*a*s, which have of course naturally evolved to be optimized for absorption of the available solar energy, are of considerable interest for use in solar-collection/energy-conversion schemes.

The optical properties[15,16] of N-confused porphyrins (NCPs)[17] are in many ways similar to chlorins, yet the synthesis of these molecules is much more straightforward.[18,19] Two N-confused tetraphenylporphyrin (NCTPP) tautomers (**1e** and **1i** in Figure 1) are observed in solution. One tautomer (**1e**) has an external N−H group and appears to be stabilized in highly polar solvents, presumably by hydrogen bonding with the solvent,[17] while the second tautomer (**1i**) has two internal N−H groups and is preferred in less polar (aromatic and halogenated) solvents. The absorption spectra of both tautomers display Soret ($S_0 \rightarrow S_2$) and Q-band ($S_0 \rightarrow S_1$) transitions that are significantly red-shifted and, in the case of the Q-bands, more intense than tetraphenylporphyrin (H_2TPP).[15−17] These optical features have been attributed[15,16,20] to a break in the degeneracy of the two sets of interacting orbitals used in the Gouterman four-electron, four-orbital model,[21] where the formerly forbidden Q-band transitions ($S_0 \rightarrow S_1$) become quasi-allowed.

We recently investigated the excited state dynamics of NCPs **1e** and **1i** using femtosecond and picosecond time-resolved spectroscopy,[16] and the excited state potential energy surface using time-dependent density functional (TD-DFT) calculations. In the present work, we examine the absorption spectra of the one-electron oxidized and reduced radical ions of N-confused tetraphenylporphyrins **1i** and **1e** using spectroelectrochemistry and calculations at the density functional level of theory. The rapid rate of the electrochemical processes in the thin-layer spectroelectrochemical cell, as well as the information obtained from both the redox potentials and the resulting absorption spectra, makes thin-layer spectroelectrochemistry ideal for these experiments. Diffusion of the reactive intermediates generated within the thin-layer chamber is negligible, and so the spectral characterization of the reactive (oxidized/reduced) intermediates can be readily determined.[22] The radical cations of these molecules are particularly interesting since they are similar to those formed in biological systems upon the one-electron oxidation occurring in both respiration[23,24] and photosynthesis.[6]

II. EXPERIMENTAL SECTION

Spectroelectrochemistry. Thin-Layer UV−vis spectroscopy (TL-UV−vis) and thin-layer spectrocoulometry (TL-SC) spectra were obtained using an Ocean Optics USB2000+F0009 UV−vis spectrophotometer. The optical instrument was equipped with a DT-Mini 2 deuterium−tungsten light source and a BASi SEC-C thin-layer quartz glass spectroelectrochemical cell, which was in turn connected to a BASi Epsilon potentiostat−galvanostat. Thin-layer cyclic voltammetry (TL-CV) experiments were performed without the UV−vis spectrophotometer and were run at dE/dt =50 mV/s. The SEC-C cell employed for electrochemical (CV) or optical experiments (TL-UV−vis and TL-SC) was constructed in a typical three-electrode arrangement using a Cypress glassy carbon disk (1 mm diameter) or a BASi EF-1355 platinum-gauze as the working electrodes. Silver and platinum wires were used as pseudoreference and counter electrodes, respectively. All potentials were referenced to the ferrocinium|ferrocene redox couple (denoted as $Fc^+|Fc$).[25,26] All experiments were carried out at 298 K using N-confused tetraphenylporphyrin (NCP) solutions (840 μL of 1.62 mM electrolytic solutions) prepared in DMF or toluene (J.T. Baker). The samples contained 0.1 M Bu_4NPF_6 (Aldrich) as the supporting electrolyte, and were deoxygenated by bubbling ultrapure N_2 (Praxair) for 15 min prior to data acquisition. The solvents were dried prior to use over molecular sieves (Aldrich).

Computational Methods. Geometry optimizations were performed at the density functional level of theory (DFT) using Becke's gradient corrected three-parameter[27] exchange functional with the correlation functional of Lee, Yang, and Parr[28] (B3LYP[29]) at the 6-31G(d) basis set. All structures were confirmed to be minima by vibrational frequency analyses; zero-point vibrational energy corrections were scaled.[30] Single-point energy calculations at the B3LYP/6-31+G(d) level were performed to obtain more accurate energies with the B3LYP/6-31G(d) geometries. Structural details are provided in the Supporting Information. In order to better approximate the condensed phase experiments in both electrochemical calculations and computed absorption spectra, the gas phase B3LYP/6-31G(d) structures were subsequently optimized using the polarizable continuum model (PCM)[31] implemented in Gaussian 03.[32] Acetonitrile (ε = 36.64) was used in place of DMF (ε = 36.64) in the PCM calculations for **1e**, while toluene was used for **1i**. Absorption spectra were obtained using time-dependent (TD) DFT calculations at the TD-B3LYP/6-31+G(d)//B3LYP/6-31G(d) level in both gas and solution phases. Similarly, the computed electrochemical data were obtained in solution at the PCM-B3LYP/6-31+G(d)//B3LYP/6-31G(d) (PCM-optimized) level. All calculations were performed under either C_1 symmetry (N-confused tetraphenylporphyrins) or D_{2h} symmetry (tetraphenylporphyrins) within the Gaussian 03 software package.[32] The nomenclature used to describe the N-confused porphyrin orbitals has been described elsewhere.[2,15,20]

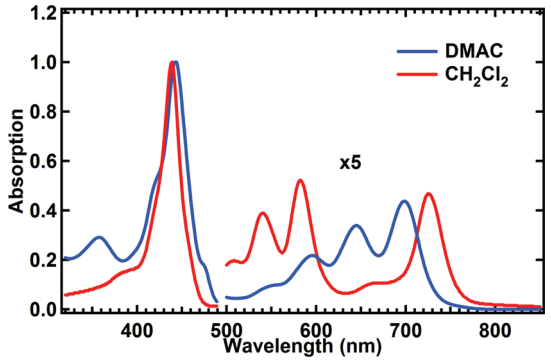

Figure 2. Absorption spectra of **1e** (DMAc, blue) and **1i** (CH_2Cl_2, red). The spectra were normalized to the Soret band maximum; the Q-band region is shown expanded above by a factor of 5.

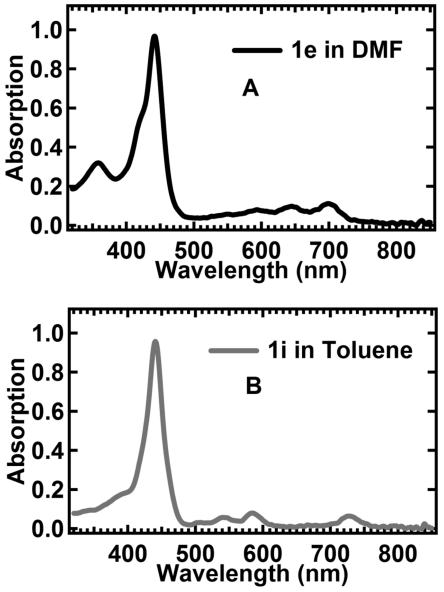

Figure 3. Thin-layer absorption spectra of **1e** (DMF, A) and **1i** (toluene, B). Both solutions contain 0.1 M Bu_4NPF_6.

III. RESULTS

Solution and Thin-Layer Absorption Spectroscopy. The steady state absorption spectra of **1i** and **1e**[17,15,16,20] in solution (Figure 2) are characterized by Soret and Q-bands that are red-shifted from H_2TPP, with the specific energies and oscillator strengths highly dependent upon the tautomer. While tautomer **1e** (in DMAc) has a strong Soret band absorption at 442 nm and a Q-band region that gains intensity with decreasing energy (Figure 2), tautomer **1i** (i.e., in CH_2Cl_2) has a Soret band at 437 nm and a Q-band structure similar to free base tetraphenylchlorin (H_2TPC), with an intense $Q_y(0,0)$ band at 724 nm as the dominant low energy feature (Figure 2).[33] The thin-layer absorption spectra shown in Figure 3 are nearly identical to those obtained in solution. The thin-layer spectrum of **1e** obtained in DMF (Figure 3A) has a Soret band at λ_{max} ~442 nm and Q-bands that are quite similar to those found in the steady state solution spectrum. Similarly, the Soret band in the thin-layer spectrum of **1i** in toluene is observed at 441 nm. The Q-band region is also similar to the spectrum obtained in CH_2Cl_2, with the low energy $Q_y(0,0)$ band appearing at 726 nm. The solution and thin-layer absorption data for both tautomers in both polar and nonpolar solvents are summarized in Table 1.

Table 1. Steady State Absorption in Bulk Solution and Thin-Layer Absorption Data for N-Confused Tetraphenylporphyrin Tautomers 1e and 1i

		Soret (nm)	Q-band (nm) ($\varepsilon \times 10^4$ M^{-1} cm^{-1})			
compound	solvent	($\varepsilon \times 10^4$ M^{-1} cm^{-1})				
1i[a]	CH_2Cl_2	437	539	580	665	724
1e[a]	DMAc	442	550	595	644	699
1i[b]	toluene	441[c]	546	581	656	726
1e[b]	DMF	442	547	593	645	699

[a] Steady state solution spectra. [b] Thin-layer spectra. [c] This band has been observed at 441 nm in a toluene solution as well (Alemán, E. A. Ph.D. Dissertation, The University of Akron, Akron, OH, 2006.).

Electrochemical Measurements. Assuming that each of the tautomeric forms of the porphyrin are the predominant form present in each of the two solvents considered, electrochemical experiments were performed to assess the redox potentials of each tautomer. The thin-layer cyclic voltammetry (TL-CV) responses for **1e** in DMF are shown in Figure 4A, while the corresponding voltammograms obtained in toluene for tautomer **1i** are shown in Figure 4B. In both voltammetric responses, the anodic and cathodic scans were recorded from the equilibrium potential, indicated by the dashed line in each voltammogram. The peaks marked with asterisks in parts A and B of Figure 4 are assigned to the well-known pseudoredox response of hydroquinone-type groups that appear on the surface of the working glassy carbon electrode.[34−36]

Inspection of the anodic responses in Figure 4 (red curves) reveals an oxidation signal for each tautomer at approximately +0.65 V for **1e** (Figure 4A) and +0.60 V for **1i** (Figure 4B). These signals represent the one-electron oxidation of the NCP to yield the corresponding radical cations, $\mathbf{1e}^{\bullet+}$ and $\mathbf{1i}^{\bullet+}$, respectively. The cathodic responses (the blue curves in Figure 4) reveal two reduction signals for each tautomer, at approximately −1.4 and −2.1 V for **1e** (Figure 4A) and −1.6 and −2.1 V for **1i** (Figure 4B). These signals are attributed to consecutive one-electron reductions of the NCP species, yielding first the radical anion $NCP^{\bullet-}$ followed by the second reduction to produce the dianion NCP^{2-}. The oxidation and reduction potentials of **1e** and **1i** in DMF and toluene, as well as those of H_2TPP and ZnTPP in similar solvents, are shown in Table 2.

Spectroelectrochemistry. Thin-layer spectrocoulometry (TL-SC) spectra were obtained by preparing the NCP solutions in DMF and toluene, polarizing the electrode at potentials at which electron transfer reactions occur, and simultaneously measuring the corresponding spectroscopic responses as a function of time. The TL-SC spectra obtained for **1e** after the first oxidation at +0.7 V is shown in Figure 5A and that of the first reduction at −1.4 V in Figure 5B. Similarly, the TL-SC spectra obtained for **1i** upon oxidation at +0.6 V is shown in Figure 6A and at the first reduction process at −1.6 V in Figure 6B.

The spectra shown in Figure 5A for the first oxidation of tautomer **1e** in DMF show depletion of the NCP absorption bands, with new absorption bands for the radical cation $\mathbf{1e}^{\bullet+}$ appearing in the Soret region at ~462 nm, and in the Q-band region at 667 and 820 nm. Well-defined isosbestic points were observed for the disappearance of the neutral NCP absorption

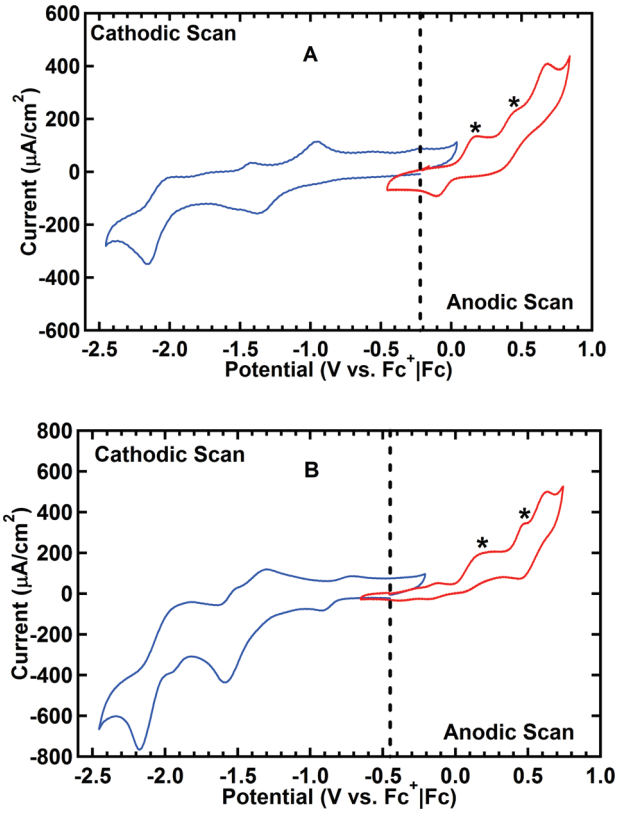

Figure 4. Thin-layer voltammograms of N-confused tetraphenylporphyrin tautomers in 0.1 M Bu_4NPF_6 solutions of **1e** in DMF (A) and **1i** in toluene (B). The anodic scans are shown in red while the cathodic scans are shown in blue. The asterisk (*) indicates positions of the pseudoredox response of hydroquinone-type groups that appear on the surface of the working glassy carbon electrode.

Table 2. Half-Wave Potentials ($E_{1/2}$) for the Oxidation and Reduction of NCPs 1e and 1i, H_2TPP, and ZnTPP in Nonpolar and Polar Solvents

compound	solvent	electrolyte	$E_{1/2}$ (ox/2)[a]	$E_{1/2}$ (ox/1)[a]	$E_{1/2}$ (red/1)[a]	$E_{1/2}$ (red/2)[a]
1i	toluene	Bu_4NPF_6		0.60	−1.64	−2.1
H_2TPP[b]	CH_2Cl_2	Bu_4NPF_6	0.82	0.52	−1.67	−1.98
ZnTPP[c]	CH_2Cl_2	Bu_4NPF_6	0.71	0.42	−1.79	
1e	DMF	Bu_4NPF_6		0.65	−1.42	−2.1
H_2TPP[d]	PhCN	Bu_4NPF_6			−1.61	−2.0
ZnTPP[e]	DMF	TBAP		0.8[f]	−1.80	−2.28

[a] Volts, referenced vs $Fc^+|Fc$. [b] Taken from: Wilford, J. H.; Archer, M. D.; Bolton, J. R.; Ho, T.-F.; Schmidt, J. A.; Weedom, A. C. *J. Phys. Chem.* **1985**, *89*, 5395−5398. [c] Taken from: Armaroli, N.; Diederich, F.; Echegoyen, L.; Habicher, T.; Flamigni, L.; Marconi, G.; Nierengarten, J.-F. *New J. Chem.* **1999**, *23*, 77−83. [d] Taken from: Inisan, C.; Saillard, J.-Y.; Guilard, R.; Tabard, A.; Le Mest, Y. *New J. Chem.* **1998**, *22*, 823−830. [e] Taken from: Kadish, K. M.; Cornillon, J. L.; Yao, C.-L.; Malinski, T.; Gritzner, G. *J. Electroanal. Chem.* **1987**, *235*, 189−207. [f] Acquired in acetonitrile vs SCE with TBAHP as the supporting electrolyte.

bands and the appearance of the radical cation absorption bands. The TL-SC spectra appearing at the first reduction of **1e** in DMF (Figure 5B) also show a decrease in the intensity of the N-band at ∼357 nm, as well as a slight shift in the Soret band to lower

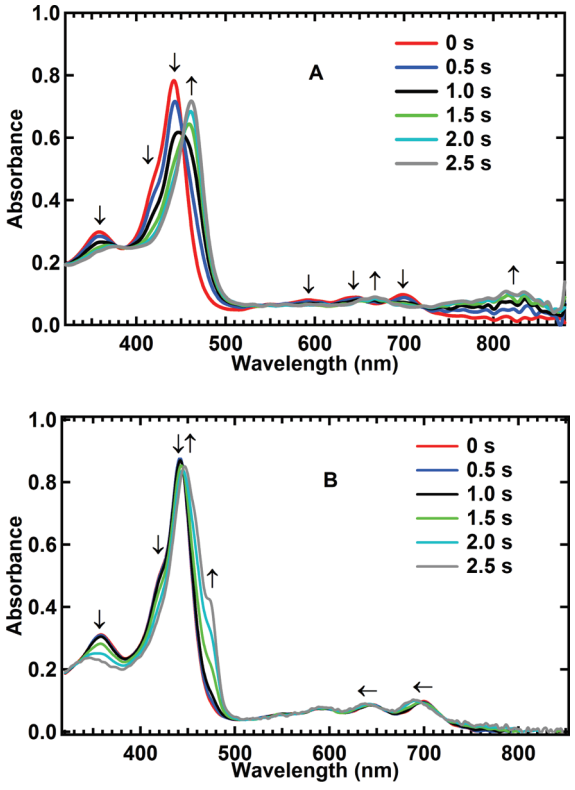

Figure 5. Thin-layer spectrocoulometry spectra of NCP **1e** in DMF obtained for the first oxidation at +0.7 V (A) and the first reduction at −1.4 V (B).

energy (447 nm) with the concomitant growth of a shoulder to the red at 473 nm. The two low-energy Q bands in $\mathbf{1e}^{\bullet-}$ are blue-shifted to 636 and 690 nm, while the higher energy bands at 550 and 595 nm do not change appreciably.

The spectra obtained upon oxidation of tautomer **1i** in toluene (Figure 6A) show a decrease of the absorption bands of neutral **1i** consistent with the depletion of the ground state NCP, as well as the growth of new absorption bands appearing at ∼460 nm (Soret) and 659 and 805 nm (Q-band), and a very small band ∼400 nm. Well-defined isosbestic points were observed for all of the neutral and radical cation absorption bands. The spectra observed upon reduction of **1i** in toluene (Figure 6B) display a clear depletion of the starting compound, with a decrease of the Soret band at 440 nm, and noticeable decreases in the intensity of the $Q_x(0,0)$ band at 583 nm and the low energy $Q_y(0,0)$ band at 724 nm. A new absorption band in the Soret region appears at 454 nm with a weak shoulder to the red at 472 nm. New absorption bands are also found in the N-band region at ∼340 nm and in the Q-band region at 635 and 683 nm, and the Q-bands at 543 and 581 nm shift to ∼546 and ∼590 nm, respectively. Isosbestic points were observed for the Q-band transitions. The changes in the absorption spectrum are attributed to formation of $\mathbf{1i}^{\bullet-}$. These data, together with the existing spectroelectrochemical data for the radical anions and cations of H_2TPP, ZnTPP, and the tetraphenylchlorins H_2TPC and ZnTPC, are shown in Table 3.

Computational Results. Time-dependent density functional calculations have shown[20] that the unoccupied b_{2g} and b_{3g} orbitals of **1e** are split to higher and lower energies relative to the analogous and nearly degenerate b_{2g} and b_{3g} orbitals of H_2TPP, while both the occupied b_{1u} and a_u orbitals increase in energy relative to those in H_2TPP. In tautomer **1i**, the degeneracy of the

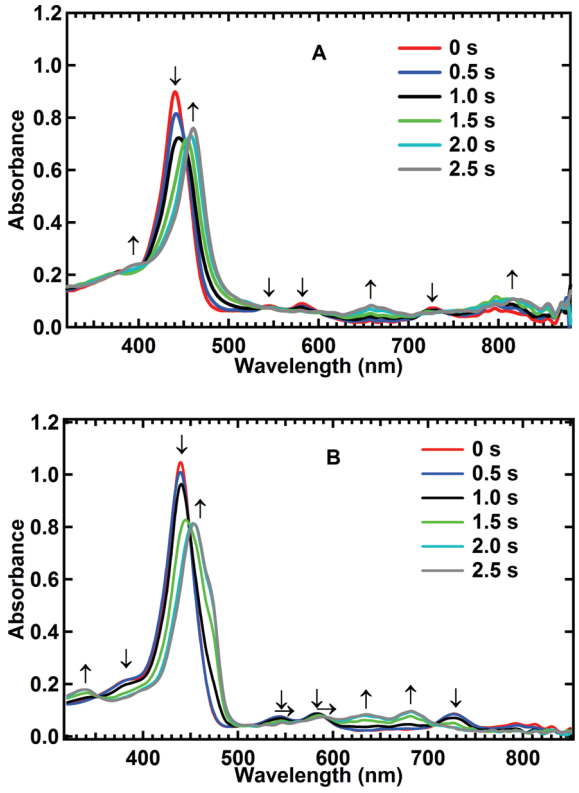

Figure 6. Thin-layer spectrocoulometry spectra obtained for the first oxidation at +0.7 V (A) and the first reduction at −1.6 V (B) of N-confused tetraphenylporphyrin **1i** dissolved in toluene.

unoccupied orbitals in H_2TPP is also lifted, with both b_{2g} and b_{3g} orbitals decreasing in energy. The occupied b_{1u} orbital increases in energy relative to the analogous orbital in H_2TPP, while the a_u orbital decreases in energy. These calculations are consistent with ground state absorption experiments[15−17] that show weakly allowed and, as a result, more intense and lower energy Q-band transitions relative to H_2TPP. In the case of **1i**, the changes result in an absorption spectrum comparable to the similarly less symmetric tetraphenylchlorin (H_2TPC). These calculations are highly relevant to the present work, since formation of the singlet excited state involves promotion of the highest energy electron into the lowest energy unoccupied orbital, similar to formation of both the radical cation where the electron is removed completely and the radical anion where an additional electron is added to the molecule.

A. Geometry Optimizations. The geometries of the neutral, oxidized, and reduced forms of NCPs **1i**, **1e**, and free-base porphyrin H_2TPP were optimized at the B3LYP/6-31G(d) level of theory under C_1 symmetry. The geometries of NCPs of neutral **1i** and **1e** calculated here are consistent with experiment[17] and our earlier calculations.[15,20] The N-confused A ring in **1i** (Figure 1) has been shown to cant significantly out of the plane of the macrocycle[37] as a result of the steric congestion caused by the presence of the extra hydrogen in the center of the ring. In contrast, the macrocycle in NCP **1e** is largely planar. The phenyl rings in both compounds are twisted out of plane and are oriented in a geared relationship with respect to one another.

As expected, the geometries of both the reduced ($\mathbf{1e}^{\bullet-}$, $\mathbf{1i}^{\bullet-}$) and oxidized ($\mathbf{1e}^{\bullet+}$, $\mathbf{1i}^{\bullet+}$) NCPs exhibit minor structural changes relative to their neutral counterparts. In general, the macrocycles of **1e** and **1i** contract slightly upon oxidation and expand slightly upon reduction. These results are not unexpected, given the nodal properties of the B_{1u} SOMO in the radical cation and the B_{3g} SOMO in the radical anion of both tautomers. The oxidized and reduced forms of H_2TPP show similar structural changes to **1e** and **1i** upon either oxidation or reduction. The macrocycle of NCP **1e** remains planar in both the oxidized and reduced electronic states. The macrocycle in **1i**, which is nonplanar to begin with, distorts further out of the plane upon oxidation to $\mathbf{1i}^{\bullet+}$, while the macrocycle of the corresponding radical anion $\mathbf{1i}^{\bullet-}$ remains largely the same as neutral **1i**. Neither oxidation nor reduction distorts the macrocycle of H_2TPP appreciably from its planar geometry. Oxidation and reduction of both NCPs also lead to rotation of the meso phenyl groups toward more planar geometries, with the

Table 3. Absorption Data for the Radical Ions of 1e and 1i, H_2TPP, ZnTPP, H_2TPC, and ZnTPC

compound	solvent	Soret (nm)	Q-band (nm)			
$\mathbf{1e}^{\bullet+}$	DMF	462	667			820
$\mathbf{1i}^{\bullet+}$	toluene	460	659			805
$\mathbf{1e}^{\bullet-}$	DMF	447[a]	595	636	690	
$\mathbf{1i}^{\bullet-}$	toluene	454[b]	590	635	683	
$H_2TPP^{\bullet+}$	CH_2Cl_2[c,d]	436	653	609	656	
$H_2TPP^{\bullet-}$	DMF[e]	405, 430 (sh), 448	625	683	765	873
$ZnTPP^{\bullet+}$	CH_2Cl_2[f]	450	600	690		850
$ZnTPP^{\bullet-}$	THF,[g] DMF[h]	445, 465	728	750		805, 910
$H_2TPC^{\bullet-}$	DMF[e]	370, 432		782		
$ZnTPC^{\bullet-}$	DMF[i]	350, 500	740	880	940	

[a] The appearance of a strong shoulder at 473 nm was also observed. [b] The appearance of a weak shoulder at 472 nm and a new N-band at 340 nm were also observed. [c] Paliteiro, C.; Sobral, A. *Electrochim. Acta* **2005**, *50*, 2445−2451. [d] Gasyna, Z.; Browett, W.R.; Stillman, M.J. *Inorg. Chem.* **1985**, *15*, 2440−2447. [e] Peychal-Heiling, G.; Wilson, G. S. *Anal. Chem.* **1971**, *43*, 550−556. [f] Fajer, J.; Borg, D. C.; Forman, A.; Dolphin, D.; Felton, R. H. *J. Am. Chem. Soc.* **1970**, *92*, 3452−3459. [g] Closs, G. L.; Closs, L. E. *J. Am. Chem. Soc.* **1963**, *85*, 818−819. [h] Recorded in a DMF/hydrazine hydrate matrix at low temperatures: Mack, J.; Stillman, M. J. *J. Porphyrins Phthalocyanines* **2001**, *5*, 67−76. [i] Fajer, J.; Borg, D. C. Forman, A.; Dolphin, D.; Felton, R. H. *J. Am. Chem. Soc.* **1973**, 2739−2741.

Table 4. Relative Gas Phase Energies (kcal mol^{-1}) of Neutral, Reduced, and Oxidized N-Confused Porphyrins (1e, 1i, $\mathbf{1e}^{\bullet-}$, $\mathbf{1i}^{\bullet-}$, $\mathbf{1e}^{\bullet+}$, and $\mathbf{1i}^{\bullet+}$), and Tetraphenylporphyrin (H_2TPP, $H_2TPP^{\bullet-}$, and $H_2TPP^{\bullet+}$) at the B3LYP/6-31G(d) and B3LYP/6-31+G(d)//B3LYP/6-31G(d) Levels of Theory

compound	B3LYP/6-31G(d)	B3LYP/6-31+G(d)// B3LYP/6-31G(d)
$\mathbf{1e}^{\bullet+}$	7.25	7.10
$\mathbf{1i}^{\bullet+}$	7.30	7.71
$H_2TPP^{\bullet+}$	0.00	0.00
$\mathbf{1e}^{\bullet-}$	12.9	13.3
$\mathbf{1i}^{\bullet-}$	6.32	7.36
$H_2TPP^{\bullet-}$	0.00	0.00
1e	18.3	18.2
1i	12.8	13.5
H_2TPP	0.00	0.00

amount of rotation dependent upon both the tautomer and the oxidation state. In the case of externally protonated tautomer **1e**, the phenyl groups in both $\mathbf{1e}^{\bullet+}$ and $\mathbf{1e}^{\bullet-}$ rotate ~2−5° to become more planar with the macrocycle. Both sets of torsional rotations are accompanied by small, but consistent, reductions in the C−C bond distance between the porphyrin meso carbon and the phenyl ring, indicating the delocalization of charge onto the phenyl rings helps to stabilize the radical ions. In the case of the internally protonated tautomer **1i**, the phenyl groups in radical cation $\mathbf{1i}^{\bullet+}$ rotate substantially (8−20°) relative to those of **1i**. The radical anion also experiences a general trend toward more planar meso phenyl groups, but to a lesser degree (~3−15°). The largest change in both $\mathbf{1i}^{\bullet+}$ and $\mathbf{1i}^{\bullet-}$, interestingly, occurs at the C_{10} carbon, where the phenyl group rotates 21° in $\mathbf{1i}^{\bullet+}$, and ~14° in $\mathbf{1i}^{\bullet-}$. The optimized geometries of $\mathbf{1e}^{\bullet-}$, $\mathbf{1i}^{\bullet-}$, $\mathbf{1e}^{\bullet+}$, and $\mathbf{1i}^{\bullet+}$ are included in the Supporting Information.

B. Energetic Considerations. The gas phase energies of neutral NCPs **1e** and **1i**, radical anions $\mathbf{1e}^{\bullet-}$ and $\mathbf{1i}^{\bullet-}$, and radical cations $\mathbf{1e}^{\bullet+}$ and $\mathbf{1i}^{\bullet+}$ and the corresponding states of H_2TPP were calculated at the B3LYP/6-31G(d) and B3LYP/6-31+G(d)//B3LYP/6-31G(d) levels and are summarized in Table 4. The relative energies of **1e** and **1i** have been examined previously,[15,16,20,38] with tautomer **1i** the more stable isomer by ~4.9 kcal mol^{-1} at the B3LYP/6-31+G(d)//B3LYP/6-31G(d) level, consistent with the results in this work. The relative gas phase energies of the oxidized tautomers are nearly equivalent to one another at both levels of theory, with $\mathbf{1e}^{\bullet+}$ more stable than $\mathbf{1i}^{\bullet+}$ by ~0.05 kcal mol^{-1} at the B3LYP/6-31G(d) level and ~0.6 kcal mol^{-1} lower than $\mathbf{1i}^{\bullet+}$ at the B3LYP/6-31+G(d)//B3LYP/6-31G(d) level. Both tautomers are less stable than $H_2TPP^{\bullet+}$ by ~7−8 kcal mol^{-1}. The energy difference between the reduced NCPs $\mathbf{1e}^{\bullet-}$ and $\mathbf{1i}^{\bullet-}$ is more substantial. At the B3LYP/6-31G(d) level, $\mathbf{1i}^{\bullet-}$ is more stable than $\mathbf{1e}^{\bullet-}$ by 6.6 kcal mol^{-1}, while the addition of diffuse functionals decreases this difference slightly to 5.9 kcal mol^{-1}. Once again, one-electron reduction of H_2TPP leads to a more stable radical anion than either NCP.

In order to examine the effects of solvation on the radical ions, calculations using the polarization continuum model (PCM) were performed using either toluene or CH_3CN. The calculations performed at the B3LYP/6-31+G(d) geometry on the PCM-optimized B3LYP/6-31G(d) geometries will be discussed here. Comparison of **1i** in toluene and **1e** in CH_3CN resulted in **1e** becoming more stable than **1i** by ~3.5 kcal mol^{-1}, a reversal of the gas phase calculations. Solvation also substantially changed the energy differences in both sets of radical ions. Thus, radical cation $\mathbf{1e}^{\bullet+}$ was found to be more stable than $\mathbf{1i}^{\bullet+}$ by 9.1 kcal mol^{-1} and $\mathbf{1e}^{\bullet-}$ was more stable than $\mathbf{1i}^{\bullet-}$ by 8.2 kcal mol^{-1}. The changes in stability are primarily the result of the preferential stabilization of all three oxidation states of **1e**, and in particular the radical ions, in the more polar solvent.

Interestingly, comparison of the two tautomers in the *same* solvent restored the original energetic ordering for both sets of tautomers. In toluene, the energy of **1i** was found to be more stable than **1e** by 2.8 kcal mol^{-1} while in CH_3CN the energy difference was 1.7 kcal mol^{-1}. Calculations in the more polar solvent DMSO also favored **1i**, in this case by ~1.6 kcal mol^{-1}. Calculations of the radical anions in each solvent indicated similar trends, with $\mathbf{1i}^{\bullet-}$ more stable than $\mathbf{1e}^{\bullet-}$ in toluene by 3.4 kcal mol^{-1} and in CH_3CN by 2.5 kcal mol^{-1}. The value calculated in DMSO is again the smallest and shows $\mathbf{1i}^{\bullet-}$ to be more stable by 2.2 kcal mol^{-1}. The calculated differences between the radical cations was quite small (<1 kcal mol^{-1}), although $\mathbf{1e}^{\bullet+}$ was found to be favored slightly in toluene (~0.6 kcal mol^{-1}), and $\mathbf{1i}^{\bullet+}$ favored by the same amount in the other two solvents.

C. Electronic Structures. The molecular orbitals of the NCPs **1i** and **1e** and their oxidized and reduced analogues calculated in this work are similar to those reported previously[15,20] and are included in the Supporting Information. In general, only the four frontier orbitals, LUMO+1 (b_{2g}), LUMO (b_{3g}), HOMO (b_{1u}), and HOMO-1 (a_u), are considered in the Gouterman four-electron, four-orbital model. Removal or addition of an electron, however, produces a singly occupied orbital that changes the orbital hierarchy. In addition, we have previously found that contributions from the π electrons of the phenyl rings are significant for NCPs deeper in the energetic manifold.[20] For the neutral NCPs, **1i** was found to have HOMO-2 and HOMO-3 orbitals that are of b_{2g} symmetry, while the corresponding orbitals for **1e** are of b_{2u} and b_{3g} symmetry, respectively. The general appearance of the two occupied and two unoccupied frontier orbitals in the radical ions are unchanged from that of the parent NCP, except for moving up (radical cations) or down (radical anions) in the orbital register.

The singly occupied molecular orbital (SOMO) in radical cations $\mathbf{1e}^{\bullet+}$ and $\mathbf{1i}^{\bullet+}$ arises upon removal of the electron from the HOMO, which is largely localized on the macrocycle and has b_{1u} symmetry in both tautomers. A significant amount of electron density is delocalized onto the phenyl groups in $\mathbf{1i}^{\bullet+}$, and to a lesser extent $\mathbf{1e}^{\bullet+}$, consistent with the shorter phenyl−meso-carbon bond lengths apparent in the radical cations. The singly occupied orbital in the radical anion of tautomers $\mathbf{1e}^{\bullet-}$ and $\mathbf{1i}^{\bullet-}$ results from the addition of an electron into the LUMO (b_{3g}), and the resulting SOMO therefore has b_{3g} symmetry. The reduced tautomers also show delocalization of the singly occupied orbital onto the phenyl rings, but to a much smaller extent than is observed for $\mathbf{1i}^{\bullet+}$, consistent with the smaller changes in bond lengths at the meso-carbon−phenyl bond. In the two tautomers of the radical cation, the remaining four orbitals are the same with LUMO+1 (b_{2g}), LUMO (b_{3g}), HOMO (a_u), and HOMO-1 (b_{2g}), while the four orbitals in the radical anion tautomers are in LUMO+1 (a_u), LUMO (b_{2g}), HOMO (b_{1u}), and HOMO-1 (a_u) symmetry.

IV. DISCUSSION

Interpretation of Electrochemical and Spectroelectrochemical Results for NCPs 1i and 1e, and Comparison with H_2TPC, H_2TPP, and ZnTPP: Experiment and Calculations. *A. Electrochemistry.* The oxidation and reduction properties of NCP tautomers **1i** and **1e** were determined in toluene and DMF vs the $Fc^+|Fc$ redox couple using cyclic voltammetry (CV). In toluene, the oxidation potential of **1i** was found to be 0.60 V, which is slightly higher than either H_2TPP or ZnTPP under similar conditions. The first oxidation waves for H_2TPP and ZnTPP have oxidation potentials at 0.52 V[39] (H_2TPP) and 0.42 V[40] (ZnTPP) in CH_2Cl_2 vs $Fc^+|Fc$.[41] Unlike **1i**, however, removal of a second electron to form the dication is known to occur for both ZnTPP and H_2TPP in nonpolar solvents ($Fc^+|Fc$: 0.82 V for H_2TPP and 0.71 V for ZnTPP in CH_2Cl_2; SCE: ~1.25−1.36 V for H_2TPP and ~1.14 V for ZnTPP).[42] Although we did not perform product studies on these oxidations, it is possible that formation of the dication in **1i** is accompanied by decomposition or chemical reaction, thereby preventing its direct observation. The oxidation potential of tautomer **1e** in DMF is similar to that determined for **1i** in CH_2Cl_2, with E_{ox} 0.65 V. Oxidation potentials under the

experimental conditions used here are not available for comparison to H_2TPP or ZnTPP in polar solvents. However, experiments in polar solvents with the same supporting electroyte used here (Bu_4NPF_6) have been performed, with oxidation of H_2TPP occurring at potentials of between 1.08[43] and 1.25[44] V in DMF (vs SCE), and ZnTPP oxidizing at 0.93 V (in benzonitrile vs SLCE).[45] These values correlate, after correction to the $Fc^+|Fc$ reference electrode,[46] to potentials of E_{ox} ~0.63−0.80 V for H_2TPP and ~0.48 V for ZnTPP vs $Fc^+|Fc$. The first oxidation potential of the less symmetric and related tetraphenylchlorin (H_2TPC) has been determined to be E_{ox} ~0.90 in DMF against the SCE reference electrode.[43] After correcting[46] for the reference electrode potential (SCE vs $Fc^+|Fc$), the oxidation potential of H_2TPC is estimated to be E_{ox} ~ 0.42 V ($Fc^+|Fc$). The oxidation potentials of **1e** and **1i** are thus comparable to the literature reported values of similar porphyrins.

The reduction of NCPs **1i** and **1e** was also performed in toluene and DMF, with the first reduction potential occurring at −1.6 V for **1i** in toluene, and −1.4 V for **1e** in DMF. The second reduction potential for both **1i** and **1e** was observed at −2.1 V. The first reduction potentials of H_2TPP and ZnTPP in CH_2Cl_2 ($Fc^+|Fc$, Bu_4NPF_6)[47,48] have been reported at slightly more negative potentials of −1.67 V[39] and −1.79 V,[49] respectively. A second reduction wave was observed for H_2TPP under these conditions at −1.98 V. In the more polar benzonitrile, H_2TPP was found to reduce at −1.61 and −2.0 V[50] ($Fc^+|Fc$, Bu_4NPF_6) while ZnTPP was reduced at −1.80 and −2.28 V, ($Fc^+|Fc$, Bu_4NClO_4). The reduction potentials of **1i** and **1e** are therefore quite comparable to those of H_2TPP under similar conditions and are reduced at slightly less negative potentials than ZnTPP.

The reduction potentials of the less symmetric H_2TPC have been determined in DMF using the SCE reference electrode, with the first reduction potential at −1.12 V and the second potential at −1.52 V.[51] After correcting[46] to the $Fc^+|Fc$ reference electrode used in this work, the reduction potential of H_2TPC is estimated to be E_{red} −1.57 V. The reduction potential for H_2TPP was also determined in the earlier work[51] and was, for comparison, found to be −1.08 V vs SCE, or −1.53 V after correction for the $Fc^+|Fc$ electrode. Thus, the ordering of the reduction potentials between the four free base compounds against the $Fc^+|Fc$ reference electrode is: **1e** < **1i** < H_2TPP < H_2TPC.

In order to better understand the redox properties of NCPs **1e** and **1i**, the oxidation (E_{ox}) and reduction (E_{red}) potentials of each tautomer, as well as H_2TPP and H_2TPC, were computed in both polar (DMF) and nonpolar (toluene) solvents using the PCM model in Gaussian 08 and then compared to the corresponding experimental redox potentials. The calculations were performed using the Born−Haber cycle (Scheme 1, eq 1), where the standard Gibbs free energy

$$\Delta G^{0,\,redox}_{solv} = \Delta G^{0,\,redox}_{g} + \Delta G^{0}_{s}(Red) + \Delta G^{0}_{s}(Ox) \quad (1)$$

of the redox half reaction ($\Delta G^{0,redox}_{solv}$) consists of the free energy change in the gas phase ($\Delta G^{0,redox}_{g}$) as well as the solvation free energies of the oxidized ($\Delta G^{0}_{s}(Ox)$) and reduced species ($\Delta G^{0}_{s}(Red)$). This method has been shown to be reasonably successful at predicting the redox properties of organic redox reactions using solvation models such as the polarizable continuum model (PCM).[52] Calculations at the PCM-B3LYP/6-31+G(d)//B3LYP/6-31G(d) level yielded the redox potentials shown in Table 5 after correction to the $Fc^+|Fc$ electrode.[53] The benchmark values for H_2TPP (−1.516 in DMF and −1.777 in toluene) and

Scheme 1

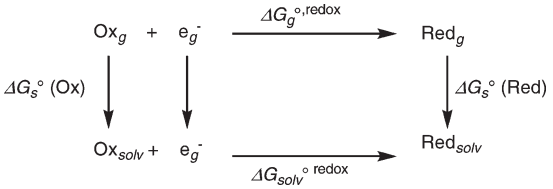

Table 5. Computed and Experimental Half-Wave Potentials for the Oxidation (E_{ox}) and Reduction (E_{red}) of NCPs 1e and 1i, H_2TPP, and H_2TPC in Nonpolar and Polar Solvents

compound	solvent[a]	E_{ox} (calcd)[b]	E_{ox} (expt)[c]	E_{red} (calcd)[b]	E_{red} (expt)[c]
1e	DMF	0.188	0.65	−1.414	−1.42
1i	toluene	0.426	0.60	−1.624	−1.64
H_2TPP	DMF	0.609	0.63[d,e]	−1.516	−1.61[d,f,g]
H_2TPP	toluene	0.732	0.52[h,i]	−1.777	−1.67[d,e]
H_2TPC	DMF	0.507	0.42[d,e]	−1.607	−1.57[d,j]
H_2TPC[e]	toluene	0.633	NA[k]	−1.857	NA[k]

[a] Calculated using the PCM solvent model. [b] Volts, corrected to the $Fc^+|Fc$ couple from the computed SHE. [c] Volts, referenced vs $Fc^+|Fc$. [d] See ref 43. [e] Taken from: Strauss, S. H.; Thompson, R. G. *J. Inorg. Biochem.* **1986**, *27*, 173−177. [f] Benzonitrile. [g] Taken from: Inisan, C.; Saillard, J.-Y.; Guilard, R.; Tabard, A.; Le Mest, Y. *New J. Chem.* **1998**, *22*, 823−830. [h] CH_2Cl_2. [i] Taken from: Wilford, J. H.; Archer, M. D.; Bolton, J. R.; Ho, T.-F.; Schmidt, J. A.; Weedom, A. C. *J. Phys. Chem.* **1985**, *89*, 5395−5398. [j] Taken from: Peychal-Heiling, G.; Wilson, G. S. *Anal. Chem.* **1971**, *43*, 550−556. [k] Data not available.

H_2TPC (−1.607 in DMF and −1.857 in toluene) are quite similar to the experimentally available values, indicating the calculations at this level are reasonable for predicting the E_{red} potentials of **1e** and **1i** with some confidence. The calculations for **1e**/**1e**$^{\bullet-}$ and **1i**/**1i**$^{\bullet-}$ reveal an excellent correlation with the experimental reduction potentials, with the computed values of −1.414 V (**1e**) and −1.624 V (**1i**) identical, within experimental error, to the experimentally determined values of −1.42 and −1.64 V.

The corresponding computed oxidation potentials (E_{ox}) of H_2TPP, H_2TPC, **1e**, and **1i** were determined in DMF and toluene and are also listed in Table 5. The computed values of H_2TPP and H_2TPC in DMF (0.609 and 0.507 V, respectively) are quite close to the experimental values of 0.63 V[42,43] (H_2TPP, corrected to $Fc^+|Fc$) and 0.42 V[42] (H_2TPC, corrected to $Fc^+|Fc$). In toluene, the E_{ox} value computed for H_2TPP was 0.21 V higher than the experimental value of 0.52 V.[39] The experimental value for H_2TPC in a nonpolar solvent has not yet been reported. On the basis of the calculations for H_2TPP and H_2TPC, the experimental value of **1e** in DMF was expected to be more accurately reproduced than that of **1i** (in toluene). In fact, neither computed value matches well with the corresponding experimental value. The calculated and experimental values of **1i** differ by 0.174 V while those of **1e** differ by 0.462 V. It is unclear why these values are so far off from the experimental values.

The electron affinities (EA) of **1i**, **1e**, H_2TPP, and H_2TPC were computed (Table 6) to complement the redox calculations. The calculations were performed at the B3LYP/6-31+G(d)//B3LYP/6-31G(d) level of theory in the gas phase, and using the polarizable continuum model (PCM-B3LYP/6-31+G(d)//B3LYP/6-31G(d)) to better model the structural changes occurring upon reduction or

Table 6. Calculated Electron Affinities (EA) and Ionization Potentials (IP) of N-Confused Porphyrins 1e and 1i, as Well as those of Tetraphenylporphyrins H_2TPP and Tetraphenylchlorin H_2TPC Computed at the B3LYP/6-31+G(d)//B3LYP/6-31G(d) Level of Theory in Both the Gas Phase and Using a Polarizable Dielectric Continuum

compound	EA/eV[a] (gas phase)	EA/eV (acetontrile)[b]	EA/eV (toluene)[c]	IP/eV (gas phase)[d]	IP/eV (acetontrile)[b]	IP/eV (toluene)[c]
1e	1.852	3.177[a]		5.736	4.795	
1i	1.889		2.967	5.974		5.036
H_2TPP	1.676	3.079	3.078	6.207	5.224	5.351
H_2TPC	1.618	2.998	2.734	6.115	6.717	6.445

[a] Calculated using the equation: EA = $E(P) - E(P^{\bullet -})$, where P represents the porphyrin/porphyrinoid. [b] Acetonitrile, ε = 36.64. [c] Toluene, ε = 2.379. [d] Calculated using the equation: IP = $E(P^{\bullet +}) - E(P)$, where P represents the porphyrin/porphyrinoid.

oxidation. Toluene was again used as the nonpolar solvent and acetonitrile was used in place of DMF for a polar solvent. The relationship between reduction potential and electron affinity is defined in eq 2

$$E_{red} = \text{EA} + \text{constant} \quad (2)$$

where higher EA values correspond to less negative reduction potentials. In general, the gas phase EA values correspond quite well with the experimental and computed E_{red} values. The calculated EA value for H_2TPP was found to be 1.676 eV, in excellent agreement with the experimentally determined EA of 1.69 eV.[54] The gas phase EA calculations resulted in an order of **1i** (1.889 eV) > **1e** (1.852 eV) > H_2TPP (1.676 eV) > H_2TPC (1.618 eV). Inclusion of the polarizable continuum model in the calculations leads to a slight change in the order of the EAs: **1e** > H_2TPP > **1i** > H_2TPC, in excellent agreement with the experimental E_{red} data (eq 2). Optimization of the geometries of each compound in the dielectric continuum followed by single point calculations with diffuse functions (i.e., PCM-B3LYP/6-31+G(d)//PCM-B3LYP/6-31G(d)) provides a slightly better correlation with the solution phase experiments, with the same reduction order but with the H_2TPP and **1i** values closer together to one another in energy. The correlation between the EAs and the computed reduction potentials discussed previously is quite good.

The ionization potentials (IPs) of each compound were also calculated using DFT at the same levels of theory as the EA calculations. The calculated gas phase IP for H_2TPP of 6.207 eV matches quite well with the experimental value of 6.32 eV.[55] The analogous value for H_2TPC has not yet been determined, although bacteriochlorins are known to oxidize more readily than their porphyrinic counterparts.[56] The gas phase IP calculations shown in Table 6 indicate an apparent order of **1e** (5.736 eV) < **1i** (5.974 eV) < H_2TPC (6.115 eV) < H_2TPP (6.207 eV). Inclusion of the polarizable continuum model in the calculations does not change this ordering, although the relative energies are altered somewhat. IPs can be converted into approximate E_{ox} potentials using the relationship IP = (E_{ox}' + 4.4),[57] where E_{ox}' is the oxidation potential against the Ag/AgCl reference electrode.[58] After correction to the $Fc^+|Fc$ reference electrode used here, the E_{ox} values obtained in this way have the same general order as those calculated using the Born−Haber cycle (**1e** < **1i** < H_2TPC < H_2TPP) and are therefore different than the experimental values, where H_2TPP and H_2TPC are both slightly more easily oxidized than either **1e** or **1i**.

B. Spectroelectrochemistry. The absorption spectrum of $\mathbf{1i}^{\bullet +}$ is characterized by the disappearance of the Soret and Q-band absorptions of **1i** (Figure 6A), the concomitant increase of a new Soret-type band at 460 nm, and the appearance of new Q-band absorption at 659 nm and an absorption in the near-IR at 805 nm. Oxidation of **1e** to $\mathbf{1e}^{\bullet +}$ produces similar changes in the absorption spectrum of this tautomer, with the disappearance of the Soret band at 442 nm accompanied by the appearance of the Soret band of the radical cation at 462 nm (Figure 5A). In addition, the Q-bands of **1e** disappear and are replaced by the appearance of the new absorption bands for $\mathbf{1e}^{\bullet +}$ at 667 and 820 nm. Interestingly, when **1** is dissolved in nitrobenzene and exposed to ambient room light, the Soret band decreases significantly in intensity and a new band appears at 459 nm, while an intense band at ~811 nm is observed to appear in the Q-band region. The appearance of these new bands presumably results from the formation of $\mathbf{1e}^{\bullet +}$ produced by an exergonic photoinduced electron-transfer from electronically excited **1e** to the solvent. Paliteiro and Sobral[59] have reported a similarly large red shift for the Soret band (from 416 to 436 nm) upon oxidation of H_2TPP in CH_2Cl_2 as well as a change in the structured Q-band region where the Q(1,0) and Q(0,0) bands of the porphyrin were replaced by a broader and significantly more intense absorption band of the radical cation centered at 653 nm.[59] Solid-state experiments in tetrachloroethane matrices showed similar results.[60] In the case of ZnTPP, oxidation in CH_2Cl_2 resulted in a red shift of the Soret band from 419 to 450 nm, while the Q-band peaks of the neutral at 548 and 585 nm disappeared and were replaced by broadened bands at 600 and 690 nm, and a new weak, low energy band in the near-IR region at ~850 nm.[61]

The Soret band in the absorption spectrum obtained upon the reduction of **1i** to $\mathbf{1i}^{-}$ in toluene (Figure 6B) is red-shifted from the 441 nm observed for the neutral to 454 nm and is accompanied by the appearance of a small shoulder at 472 nm. In the Q-band region of **1i**, the low energy $Q_y(0,0)$ band at 724 nm disappears together with the $Q_x(0,0)$ band at 580 nm. Three new bands appear in the Q-band region of the spectrum at 545, 635, and 683 nm. The lower intensity Q-bands in neutral **1i** at 540 and 665 nm are underneath the emerging bands in the Q-band region of the radical cation, and their disappearance is consequently not observed. The absorption spectrum of $\mathbf{1e}^{\bullet -}$ in DMF, on the other hand, remains relatively unchanged from that of neutral **1e**, with the only observed changes being a red-shifted Soret band from 442 to 447 nm, the appearance of a shoulder on the Soret band at 472 nm, and a blue shift in the two low energy Q-band absorption peaks from 644 and 699 nm to 636 and 690 nm. The absorption spectra of the analogous H_2TPP and ZnTPP radical anions have been characterized, albeit with some difficulty because of the propensity for protonation in these compounds at the methine carbons. The absorption spectrum of $H_2TPP^{\bullet -}$ in DMF is characterized by three strong bands in the Soret region at 405, 430 (shoulder), and 448 nm, and weaker bands in the Q-band region (625, 683, 705 (shoulder), 765, and 873 nm).[51,62] The strong absorptions at 445 and 465 nm correspond to new Soret band transitions, while the weaker bands at 728 (sh), 750, and 805 nm (sh) were assigned to the new Q-band transitions of

dx.doi.org/10.1021/jp200411q |J. Phys. Chem. A 2011, 115, 6456–6471

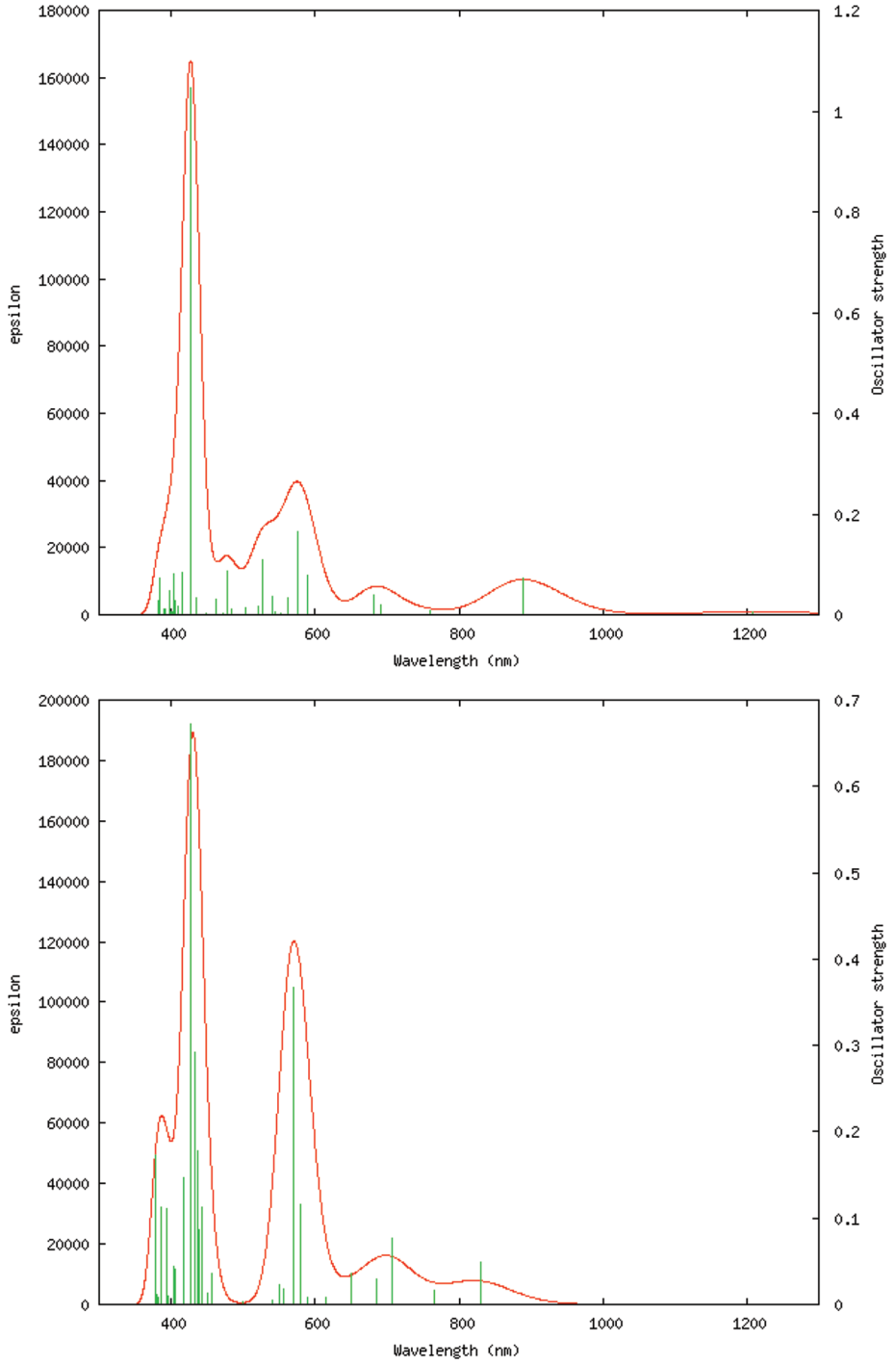

Figure 7. Computed absorption spectra for the oxidized N-confused tetraphenylporphyrins $\mathbf{1e}^{\bullet+}$ (top) and $\mathbf{1i}^{\bullet+}$ (bottom). Spectra were calculated at the TD-B3LYP/6-31+G(d)//B3LYP/6-31G(d) levels using the PCM solvation model (acetonitrile and toluene, respectively) for both calculations.

the radical anion.[63] Absorption bands at 538 nm and in the near-IR at 910 nm were both identified as arising from $\pi^* \rightarrow \pi^*$ transitions.[63] The analogous free base and zinc tetraphenylchlorin radical anions have also been characterized, with the absorption spectrum of the tetraphenylchlorin radical anion in DMF having new bands at 370, 432, and 782 nm.[51] The absorption spectrum of the radical anion of zinc tetraphenylchlorin[64] in DMF is in turn characterized by a new absorption band in the Soret region at 500 nm, as well as a new band at 740 nm and new bands in the near-IR at 880 and 940 nm. The overall changes observed here in the absorption spectra of oxidized and reduced **1i** and **1e** are therefore consistent with prior experimental results on similarly oxidized and reduced regular free-base and metallo tetraphenylporphyrin and tetraphenylchlorin. In order to better understand the experimental absorption experiments, time-dependent DFT calculations at the TD-B3LYP/6-31+G(d)//B3LYP/6-31G(d) level were performed on the radical ions of **1e** and **1i**.

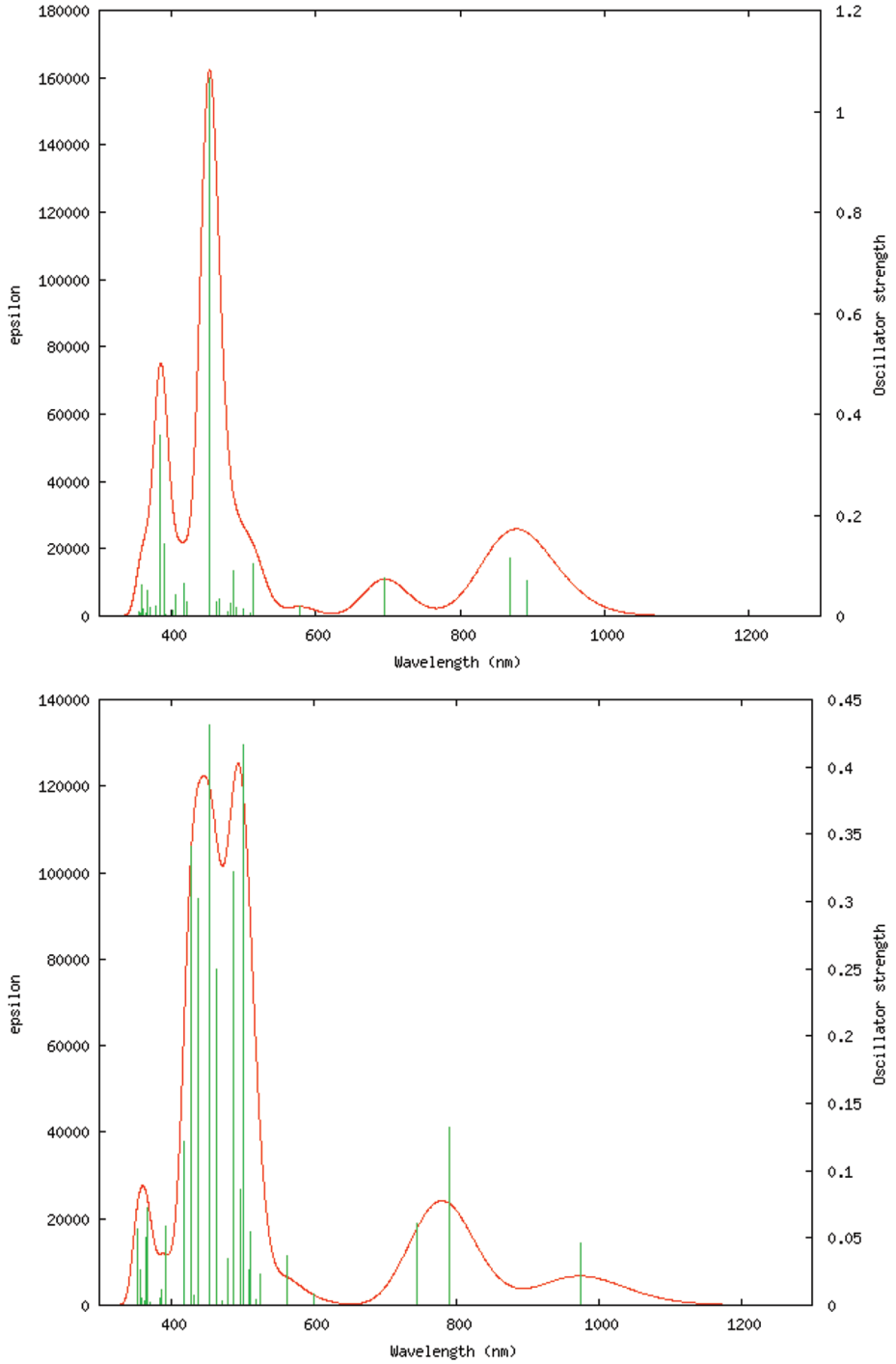

Figure 8. Computed absorption spectra for the reduced N-confused tetraphenylporphyrins $\mathbf{1e}^{\bullet-}$ (top) and $\mathbf{1i}^{\bullet-}$ (bottom). Spectra were calculated at the TD-B3LYP/6-31+G(d)//B3LYP/6-31G(d) levels using the PCM solvation model (acetonitrile and toluene, respectively) for both calculations.

C. Electronic Absorption Calculations and Comparison with Experimental Spectra. The absorption spectra of free-base porphyrins are characterized by two sets of absorption bands: (1) the low energy $S_0 \rightarrow S_1$ transitions (Q-bands) that are nearly forbidden by parity rules as a result of the high D_{2h} symmetry in free-base porphyrins (D_{4h} in metalloporphyrins), and (2) the more intense, higher energy allowed $S_0 \rightarrow S_2$ transition (the Soret or B-band). In the Gouterman four-orbital, four-electron model,[21] the Q-band transitions are represented as linear combinations of the $b_{1u}-b_{2g}/a_u-b_{3g}$ (Q_x) and $b_{1u}-b_{3g}/a_u-b_{2g}$ (Q_y) transitions.[65] The Q-band transitions are further split by vibronic coupling and are consequently observed in free-base porphyrins such as H_2TPP as a pair of bands, with each primary band, $Q_x(0,0)$ and $Q_y(0,0)$, having a higher energy ($Q_x(1,0)$ and $Q_y(1,0)$) vibrational overtone. The Soret band is an allowed transition composed of a linear combination of the a_u-b_{3g} and $b_{1u}-b_{2g}$ transitions.[65f,66,67] The intensity of this peak is found experimentally to be significantly larger than the Q-band transitions, with extinction coefficients on the order

Table 7. Calculated and Experimental Absorption Data (TD-B3LYP/6-31+G(d)//B3LYP/6-31G(d)) for the Radical Ions of N-Confused Tetraphenylporphyrin Tautomers 1e and 1i in the Gas and Solution Phases

compound	Soret (nm) (oscillator strength)[a]	Q-band (nm) (oscillator strength)[a]		near-IR (nm) (oscillator strength)[a]
$\mathbf{1e}^{\bullet+}$ (CH_3CN)	428 (100)	576 (10)	683 (3.6)	890 (6.9)
$\mathbf{1e}^{\bullet+}$ (gas phase)	417 (100)	581 (14)	696 (5.2)	906 (12)
$\mathbf{1e}^{\bullet+}$ (expt)	462		667	820
$\mathbf{1i}^{\bullet+}$ (toluene)	434 (100)	567 (51)	699 (11)	830 (7.3)
$\mathbf{1i}^{\bullet+}$ (gas phase)	410 (100)	567 (51)	699 (11)	832 (6.6)
$\mathbf{1i}^{\bullet+}$ (expt)	460		659	805
$\mathbf{1e}^{\bullet-}$ (CH_3CN)	452 (100)	578 (1.8)	696 (7.1)	870 (10)
$\mathbf{1e}^{\bullet-}$ (gas phase)	450 (100)	575 (4.5)	718 (8.6)	915 (11)
$\mathbf{1e}^{\bullet-}$ (expt)	447	595	690	
		636		
$\mathbf{1i}^{\bullet-}$ (toluene)	450 (100)	500 (97)	785 (31)	975 (11)
		563 (8.6)		
$\mathbf{1i}^{\bullet-}$ (gas phase)	448 (100)	510 (14)	785 (9.9)	1024 (4.2)
		570 (5.6)		
$\mathbf{1i}^{\bullet-}$ (expt)	454	590	683	
		635		
1e	415 (100)	579 (3.6)	702 (31)	
1i	405 (100)	581 (7.9)	646 (7.7)	

[a] The computed oscillator strengths are reported relative to the Soret band.

of $\sim 5 \times 10^5\ M^{-1}\ cm^{-1}$ for the Soret band and $\sim(5-20) \times 10^4\ M^{-1}\ cm^{-1}$ for the Q-bands. The reduction in symmetry of the macrocycle of chlorins such as tetraphenylchlorin causes the unoccupied orbitals to become nondegenerate and significantly different in energy. These energetic changes cause the b_1-c_2 and b_2-c_1 transition energies to become different, and together with the breakdown in parity rules from the changes in symmetry, result in the Q_x transition becoming significantly more intense.[15,16,33] The intensity of the Q_y transition does not change appreciably, as the b_1-c_1 and b_2-c_2 transition energies remain nearly equivalent to one another.

The four frontier orbitals of **1i** and **1e**,[20] LUMO+1 (b_{2g}), LUMO (b_{3g}), HOMO (b_{1u}), and HOMO-1 (a_u), have been previously calculated and considered in the four-electron, four-orbital model. Since the ring system is no longer symmetric in N-confused porphyrins, the previously degenerate LUMO and LUMO+1 orbitals in porphyrins having D_{4h} symmetry (the e_g orbitals) are no longer degenerate. The energetic ordering of these orbitals is nonetheless unaltered, and if the orbitals of **1i** and **1e** are approximated in the D_{4h} point group, then the frontier orbitals are similar to those of H_2TPP (e_g, e_g, b_{2u}, and a_{1u} symmetries), although orbitals deeper within the energy manifold do differ between **1e**, **1i**, and H_2TPP, with **1i** having HOMO-2 and HOMO-3 orbitals of b_{2g} symmetry, while **1e** instead has corresponding orbitals of b_{2u} and b_{3g} symmetry, respectively.

Calculations have indicated the oxidized electron in H_2TPP is removed from the b_{1u} orbital,[68] and the resulting absorption spectrum therefore likely arises from a linear combination of the promotion of the remaining electron in the new SOMO (b_{1u} symmetry) and that in the new HOMO orbital (a_u symmetry), into the nearly degenerate e_u unoccupied orbitals. In the case of **1i** and **1e**, the symmetries of the SOMOs of both radical cations (discussed earlier in the computational section) have b_{1u} symmetry, while those of the radical anions have b_{3g} symmetry. The symmetries of the LUMO and LUMO+1 orbitals are b_{2g} and a_u, respectively, for the radical anions, and b_{3g} and b_{2g} for the radical cations. Similar to the neutral precursors, the LUMO and LUMO+1 in radical ions **1i** and **1e** are not degenerate, substantially affecting the resulting absorption spectra. The optical transitions composing the absorption spectra of these radical ions are consistent with this analysis.

The simulated absorption spectra (Figures 7 and 8) for the radical ions of **1e** and **1i** were constructed using oscillator strengths calculated at the TD-B3LYP/6-31+G(d)//B3LYP/6-31G(d) level of theory using the PCM model in either acetonitrile or toluene and were fitted to Gaussian distributions with full widths at half-maxima (fwhm) of 1500 cm^{-1}. Calculations at this level were found to have a slightly better correlation with experiment than those computed in the gas phase. Although both sets of results are reported in Table 7, only the PCM calculations are discussed here. The intensities of each band are reported relative to the largest peak in the Soret band region of the spectrum (i.e., 400−440 nm). The vibrational structure of the S_1 excited-state surface cannot be determined by calculating vertical excitations, and as a result, the vibronic overtones of the Q-bands observed in the experimental spectra will not be discussed. Three bands are observed in the low-energy Q-band region of the calculated absorption spectrum of $\mathbf{1e}^{\bullet+}$ (Figure 7, top), and one in the near-IR at 890 nm with a relative intensity of 6.9. The lowest energy Q-band is calculated to arise from a pair of transitions centered at 683 nm with a relative oscillator strength of 3.6, while a higher energy and more intense Q-band is centered at 576 nm (oscillator strength ~16). A slightly less intense, higher energy band with a smaller oscillator strength (10) appears at ~526 nm. The oscillator strengths calculated for $\mathbf{1e}^{\bullet+}$ are reasonably consistent with those observed in the experimental spectrum (Table 3), although it is unclear whether the Q-band at 667 nm in the experimental spectrum should correlate with the calculated band at 576 nm or the less intense transition at 683 nm. A more intense transition (with a relative oscillator strength of 100) is observed at ~428 nm and is attributed to the radical cation Soret band. The simulated spectrum of $\mathbf{1i}^{\bullet+}$ was also determined at the TDB3LYP/6-31+G(d)//B3LYP/6-31G(d) level (Figure 7, bottom, Table 7). A low energy band at 830 nm with an oscillator strength of 7.3 is calculated in the near-IR. More prominent bands are observed in the Q-band region centered at 699 nm having a relative oscillator strength of 11, as well as a significantly more intense band (oscillator strength <51) at 567 nm. The Soret band for this radical cation is primarily composed of two intense transitions centered at 434 nm and is attributed to the overlapped $S_0 \rightarrow S_6$, $S_0 \rightarrow S_7$, and $S_0 \rightarrow S_8$ transitions. The N-band is calculated to absorb at ~385 nm (oscillator strength ~26).

The experimental spectra of radical cations $\mathbf{1e}^{\bullet+}$ and $\mathbf{1i}^{\bullet+}$ are both qualitatively more similar to the computed radical cation spectrum of $\mathbf{1e}^{\bullet+}$ in terms of overall spectral shape and the intensity pattern when fit to Gaussian distributions. The lowest energy absorption maximum at 890 nm calculated for $\mathbf{1e}^{\bullet+}$ is red-shifted 70 nm from the experimental value (820 nm), while the next lowest energy peak at 683 nm is red-shifted by 16 nm from the experimentally observed band at 667 nm. The second most intense band in the computed spectrum at 576 nm (oscillator strength 16) is not observed in the experimental spectrum, probably because it overlaps the disappearing Q-band of neutral

1e at 593 nm. The Soret band for $\mathbf{1e}^{\bullet+}$ is calculated to be blue shifted to 428 nm, 34 nm from the 462 nm experimentally determined absorption. In the case of the internally protonated tautomer $\mathbf{1i}^{\bullet+}$, the lowest energy band at 830 nm in the calculated spectrum is red-shifted 25 nm from the experimental value of 805 nm, while the next lowest energy band is red-shifted to 699 nm from the experimental value of 659 nm. The second most intense band in the computed spectrum at 567 nm is not observed in the experimental spectrum. The Soret band in this tautomer is blue-shifted to 434 nm, 26 nm from the Soret band in the experimental spectrum (460 nm).

The simulated absorption spectrum obtained from the TD-B3LYP/6-31+G(d)//B3LYP/6-31G(d) calculation of $\mathbf{1e}^{\bullet-}$ is shown in Figure 8 (top). In the near-IR region of this spectrum, the calculated band is composed of two transitions of moderate intensity centered at 870 nm and a relative oscillator strength of 10. Two bands of differing intensity are computed in the low-energy Q-band region. The lower energy Q-band is calculated to result from a single transition centered at 696 nm (oscillator strength ~7.1), while the higher energy Q-band is also composed of a much weaker transition at 578 nm (oscillator strength ~1.8). The Soret band of $\mathbf{1e}^{\bullet-}$ is calculated to arise from a single strong transition at 452 nm, with a pair of smaller bands at ~384 nm (oscillator strength ~34) that are assigned to the N-band. The calculated oscillator strengths of these bands are reasonably consistent with those in the experimental spectrum (Figure 6b). The simulated spectrum of $\mathbf{1i}^{\bullet-}$ is shown in Figure 8 (bottom). In this spectrum, the low energy band in the near-IR is moderately intense with an oscillator strength of 11 and is observed at 975 nm (Table 7). The two Q-band absorptions centered at 785 and 563 nm have relative oscillator strengths of 31 and 8.6, respectively. A distinct higher energy and very intense band is observed at ~500 nm with an oscillator strength of 97. The Soret band is composed of an overlap of the $S_0 \rightarrow S_8$, $S_0 \rightarrow S_9$, and $S_0 \rightarrow S_{10}$ transitions and has a weighted center for the band at 454 nm. A moderately intense band at 418 nm (oscillator strength ~28) is assigned to the N-band.

A comparison of the experimental and computed spectra of radical ions $\mathbf{1e}^{\bullet-}$ and $\mathbf{1i}^{\bullet-}$ indicate the experimental spectra are both qualitatively more similar to the computed spectrum of $\mathbf{1e}^{\bullet-}$ than $\mathbf{1i}^{\bullet-}$. The lowest energy Q-band absorption in the computed spectrum of $\mathbf{1e}^{\bullet-}$ at 696 nm is in excellent agreement with the corresponding bands in the experimental spectra of both $\mathbf{1e}^{\bullet-}$ (690 nm) and $\mathbf{1i}^{-}$ (683 nm). The higher energy Q-band absorptions at 636 nm ($\mathbf{1e}^{\bullet-}$) and 635 nm ($\mathbf{1i}^{\bullet-}$) in the experimental spectra presumably arise from an overtone of the 683/690 nm bands, while the 590 nm band in both experimental spectra corresponds to the weak absorption band at 578 nm in the computed spectrum. The Soret band transitions for this tautomer are extremely well-matched, with the Soret band in the calculated spectrum shifted only slightly to 450 nm from the experimentally observed values of 447 nm ($\mathbf{1e}^{\bullet-}$) and 454 nm ($\mathbf{1i}^{-}$). The relative intensities of the bands in the computed spectrum of $\mathbf{1e}^{\bullet-}$ and the experimental spectra of $\mathbf{1e}^{\bullet-}$ and $\mathbf{1i}^{\bullet-}$ are also in excellent agreement. A comparison between the computed spectrum of $\mathbf{1i}^{\bullet-}$ and the experimental spectra is not as good. In the Soret band region, the computed spectrum exhibits a split transition at 450 and 500 nm of nearly equal intensity, reasonably similar to the main experimental Soret bands at 447 nm ($\mathbf{1e}^{\bullet-}$) and 454 nm ($\mathbf{1i}^{\bullet-}$) and the related shoulders at 473 and 427 nm ($\mathbf{1e}^{\bullet-}$ and $\mathbf{1i}^{\bullet-}$). However, the low energy Q-bands predicted to occur at 785 nm are instead observed at 690 and 683 nm ($\mathbf{1e}^{\bullet-}$, $\mathbf{1i}^{\bullet-}$) in the experimental spectra. The other computed Q-band at 563 nm correlates reasonably well with the experimental band at 595 nm in both tautomers.

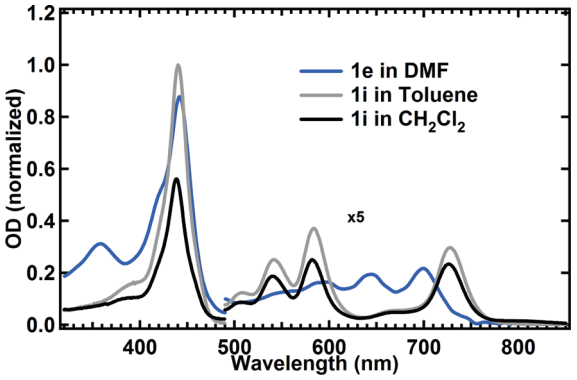

Figure 9. Overlay plot of the experimental absorption spectra of neutral N-confused tetraphenylporphyrins **1e** (DMF) and **1i** (CH_2Cl_2 and toluene).

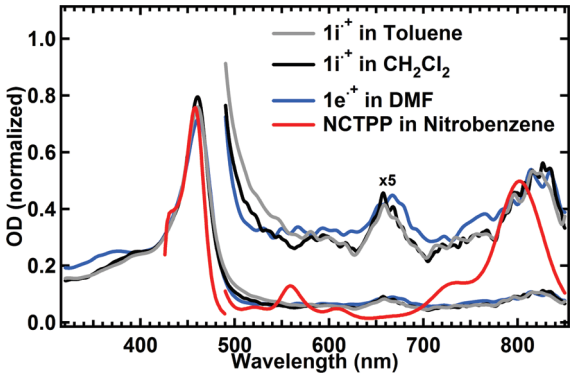

Figure 10. Overlay plot of the experimental absorption spectra of oxidized N-confused tetraphenylporphyrins $\mathbf{1e}^{\bullet+}$ (in DMF) and $\mathbf{1i}^{\bullet+}$ (in CH_2Cl_2 and toluene), and NCTPP in nitrobenzene.

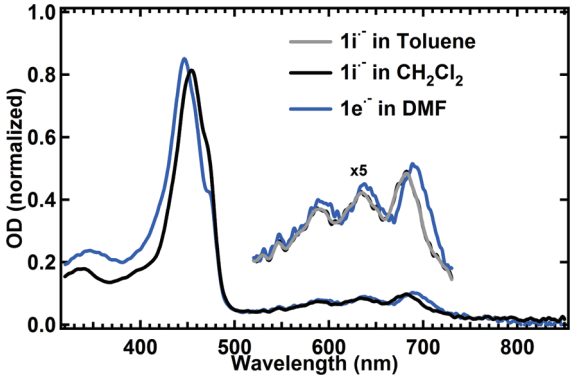

Figure 11. Overlay plot of the experimental absorption spectra of reduced N-confused tetraphenylporphyrins $\mathbf{1e}^{\bullet-}$ (in DMF) and $\mathbf{1i}^{\bullet-}$ (in CH_2Cl_2 and toluene).

Interpretation of Radical Ion Spectra. Plotting the experimental absorption spectra of neutral NCTPP in toluene, CH_2Cl_2, and DMF (Figure 9), and comparing these spectra against the similarly superimposed spectra of the radical cations in the same solvents

Table 8. Computed Energies of 1e, 1i, $1e^{\bullet+}$, $1i^{\bullet+}$, $1e^{\bullet-}$, and $1i^{\bullet-}$ in Toluene, CH_3CN, and DMSO at the PCM B3LYP/6-31G(d)//B3LYP/6-31G(d) and PCM B3LYP/6-31+G(d)//B3LYP/6-31G(d) Levels of Theory[a]

solvent	theory level	ΔH (1e−1i) kcal mol^{-1}	ΔH ($1e^{\bullet+}-1i^{\bullet+}$) kcal mol^{-1}	ΔH ($1e^{\bullet-}-1i^{\bullet-}$) kcal mol^{-1}
toluene	B3LYP/6-31G(d)//B3LYP/6-31G(d)	3.5	0.0	4.4
CH_3CN	B3LYP/6-31G(d)//B3LYP/6-31G(d)	2.5	0.8	3.3
DMSO	B3LYP/6-31G(d)//B3LYP/6-31G(d)	2.4	0.7	3.1
toluene	B3LYP/6-31+G(d)//B3LYP/6-31G(d)	2.8	−0.6	3.4
CH_3CN	B3LYP/6-31+G(d)//B3LYP/6-31G(d)	1.7	0.6	2.5
DMSO	B3LYP/6-31+G(d)//B3LYP/6-31G(d)	1.6	0.6	2.2

[a] All molecules were first optimized using the PCM solvation model in G03, and then single point calculations using the optimized geometries were performed using the same solvent.

(Figure 10) reveals an interesting result. Specifically, although the spectra of neutral **1i** (in toluene or CH_2Cl_2) and **1e** (in DMF) are distinctly different (Figure 9), the absorption spectra of the corresponding radical cations generated in these solvents (Figure 10) are quite similar to one another. Similarly, the overlaid experimental absorption spectra of the radical anions $\mathbf{1e}^{\bullet-}$ (generated in DMF) and $\mathbf{1i}^{\bullet-}$ (generated in toluene and CH_2Cl_2) are virtually identical to one another (Figure 11). These data suggest that either: (1) the absorption spectra of the radical ions (cations, anions) do not exhibit the highly solvent-dependent behavior exhibited by the neutral precursor and are, coincidentally, the same, or (2) only one tautomer is dominant in solution, irrespective of the solvent.[69]

The tautomerization between neutral **1e** and **1i** has been studied experimentally by Furuta et al.[17a] In this work, the forward direction of **1i** to **1e** in pyridine displayed values of −0.34 and −3.16 kcal mol^{-1} for ΔG^0 and ΔH^0, respectively, and had activation parameters of −14.94 and 1.93 kcal mol^{-1} for $\Delta G^{\ddagger}$ and $\Delta H^{\ddagger}$. While the pathway involved in this process has not yet been computed, the relative values of ΔH^0 are available from the calculations performed here and provide some indication of what species predominates in solution. In Table 4 we reported the energetic differences in both the gas and condensed phases, the latter using the PCM solvation model. However, these calculations do not appropriately describe the effects of solvation within *one* solvent (i.e., the equilibrium in each solvent) which are clearly important in these molecules. Therefore, calculations on the various neutral and reduced/oxidized NCPs were performed at the PCM B3LYP/6-31+G(d)//B3LYP/6-31G(d) level of theory in toluene, CH_3CN, and DMSO, and the equilibria in each solvent were then compared (Table 8). For the neutral NCPs, **1i** is favored over **1e** in all three solvents, with the value in DMSO the smallest at ∼1.6 kcal mol^{-1} and that in toluene the largest at 2.8 kcal mol^{-1}. It should be noted that these values are different from the gas-phase energies, as well as the solution-phase (PCM) energies, where we compared **1i** and **1e** with either no solvent continuum (gas phase) or in the respective solvent in which the molecule appears in solution (by NMR and UV−vis). For the radical cations, the energy differences at both theory levels are <1 kcal mol^{-1}, although $\mathbf{1e}^{\bullet+}$ is favored slightly in toluene (∼0.6 kcal mol^{-1}), and $\mathbf{1i}^{\bullet+}$ favored by the same amount in the other two solvents. For the radical anions the energy differences are more substantial, with $\mathbf{1i}^{\bullet-}$ favored in all three solvents by 2.2−3.4 kcal mol^{-1}. The computed entropic differences at the PCM B3LYP/6-31G(d)//B3LYP/6-31G(d) level for both the radical anions and radical cations are overall quite small (∼1−2 cal mol^{-1} K^{-1}) and probably do not contribute appreciably to the overall equilibria.

Interestingly, the computational data shown in Table 8 show neutral **1i** to be more stable than **1e** in all three solvents. This result is consistent with what is observed experimentally[70] in toluene and acetonitrile but is the opposite of what is observed in DMSO, for which only tautomer **1e** is observed; the reason for this apparent preference in DMSO is unclear. For the reduced tautomers, the data in Table 8 show a clear preference for $\mathbf{1i}^{\bullet-}$ in all three solvents, indicating that if an equilibrium exists between $\mathbf{1e}^{\bullet-}$ and $\mathbf{1i}^{\bullet-}$, it favors the latter radical ion. These data are consistent with the experimental absorption spectra, which are nearly identical to one another regardless of which solvent the reduction occurs in, leading us to conclude that the absorption spectra arise from the same reduced species. The computed geometries of each tautomer are not the same (since they start out in an energetic well and do not sample computational space), and the computed absorption spectra are thus not identical to one another. It is possible the two tautomers converge to a common geometry that has not been found computationally. However, such a result is not likely considering a structural change large enough to result in a common geometry midway between those of the computed radical anions would have to exist and would likely be higher in energy than those already computed. We therefore conclude that reduction in all of the solvents studied in this work is followed by isomerization to the more stable radical anion $\mathbf{1i}^{\bullet-}$. It is interesting to note that the absorption spectra of $\mathbf{1e}^{\bullet-}/\mathbf{1i}^{\bullet-}$ bear a striking resemblance to that of neutral **1e**, and it is tempting to make an analogy between the spectra of the radical anions and the neutral spectrum of **1e**. However, comparing the absorption data in Tables 1 and 8 shows the absorption bands to differ in several instances by up to 10 nm, and it is therefore more likely that the similarities are superficial, particularly since the electronic structures of the interacting Gouterman orbitals of the neutral and the radical ions are significantly different from one another.

The computational data for the oxidized tautomers (Table 8), calculated using the PCM-optimized data in the same set of solvents, shows that both forms of the radical cation are energetically similar to one another. It is therefore likely that these solutions contain an equilibrium between both tautomeric forms, although it is difficult to say with any certainty whether this is the case or whether another intermediate is present and responsible for the observed spectra. In any case, the spectra of $\mathbf{1e}^{\bullet+}$ and $\mathbf{1i}^{\bullet+}$ generated electrochemically are identical to one another as well as to the absorption spectrum obtained upon chemical oxidation in nitrobenzene.

CONCLUSIONS

The radical anion and radical cation of the two N-confused tetraphenylporphyrin tautomers **1e** and **1i** were examined using a combination of spectroelectrochemistry and computational chemistry at the density functional level. While NCP **1e** was shown experimentally to undergo oxidation at E_{ox} 0.65 V in DMF and

reduction at E_{red} −1.42 V, **1i** was oxidized in toluene at E_{ox} 0.60 V and reduced at E_{red} −1.64 V. These redox properties were computed at the B3LYP/6-31+G(d)//B3LYP/6-31G(d) level in solution using the PCM model, resulting in values of E_{ox} 0.188 V and E_{red} −1.414 V for **1e**, and values of E_{ox} 0.426 V and E_{red} −1.624 V for **1i**, all of which were very well correlated with experiment with the exception of the $\mathbf{1e}^{\bullet+}$/**1e** couple. Electron affinities and ionization potentials were computed as well and compared to the literature values for the related reference compounds H_2TPP and H_2TPC. The order of the experimental and computed reduction potentials, as well as the computed electron affinities, of **1e** and **1i** correlated well with those of the reference compounds. A similar correlation was not observed with respect to the computed ionization and computed and experimental oxidation potentials, primarily because of the outlying values for $\mathbf{1e}^{\bullet+}$.

The absorption spectra of the four radical ions were calculated using time-dependent density functional calculations at the TD-B3LYP/6-31+G(d)//B3LYP/6-31G(d) level using both gas-phase and PCM modeled geometries, and were subsequently compared to the experimental spectroelectrochemical spectra. The experimental absorption spectra of the radical anions in either solvent indicated a reasonable correlation with the computed spectra of both $\mathbf{1i}^{\bullet-}$ and $\mathbf{1e}^{\bullet-}$, while the radical cation, again generated in either solvent, showed a better correlation with the computed spectrum of $\mathbf{1e}^{\bullet+}$. Superposition of the experimental radical anion spectra showed all to be identical to one another, irrespective of solvent. Calculations of each tautomer in a variety of solvents indicated radical anion $\mathbf{1i}^{\bullet-}$ to be more stable under all conditions, and the experimental radical anion spectra were therefore assigned to this structure. Similarly, the experimental radical cation spectra were identical to one another, although the PCM calculations in the case of this species were not as definitive. The experimental spectra are, as a result, attributed to a mixture of the two tautomeric forms, which were calculated to have nearly the same energy in the several solvents examined.

■ ASSOCIATED CONTENT

Supporting Information. Optimized geometries and molecular orbitals computed at the B3LYP/6-31G(d)//B3LYP/6-31G(d) level of theory for $\mathbf{1e}^{\bullet-}$, $\mathbf{1i}^{\bullet-}$, $\mathbf{1e}^{\bullet+}$, and $\mathbf{1i}^{\bullet+}$, as well as optimized gas and solvation model Cartesian coordinates. This material is available free of charge via the Internet at http://pubs.acs.org.

■ AUTHOR INFORMATION

Corresponding Author
*E-mail: dmodarelli@uakron.edu.

■ ACKNOWLEDGMENT

D.A.M. gratefully acknowledges the support of the National Science Foundation (NSF-532057 and NSF-9816260), the Ohio Board of Regents, and The University of Akron. We also acknowledge helpful computational conversations with Professor Christopher Hadad and Mr. Shubham Vyas at Ohio State University. E.A.A. thanks the U.S. Department of Education for a GAANN fellowship. The authors also thank Dr. Shana Garrison for providing samples of **1** for use in these experiments.

■ REFERENCES

(1) See: *The Porphyrin Handbook*; Kadish, K. M., Smith, K. M., Guilard, R., Eds.; Academic Press: San Diego, CA, 2000.

(2) Gouterman, M. J. In *The Porphyrins*; Dolphin, D., Ed.; Academic Press: New York, 1978; Vol. III, pp 1−165.

(3) Kühlbrandt, W.; Wang, D. N.; Fujiyoshi, Y. *Nature* **1994**, *367*, 614.

(4) McDermott, G.; Prince, S. M.; Freer, A. A.; Hawthornthwaite-Lawless, A. M.; Papiz, M. Z.; Cogdell, R. J.; Isaacs, N. W. *Nature* **1995**, *374*, 517.

(5) Karrasch, S.; Bullough, P. A.; Ghosh, R. *EMBO J.* **1995**, *14*, 631.

(6) For recent reviews of the events occurring in the photosynthetic reaction center and light-harvesting complex, see:(a) Arnett, D. C.; Moser, C. C.; Dutton, P. L.; Scherer, N. F. *J. Phys. Chem. B* **1999**, *103*, 2014–2032. (b) Pullerits, T.; Sundström, V. *Acc. Chem. Res.* **1996**, *29*, 381–389.

(7) Amerongen, H. v.; Grondell, R. v. *J. Phys. Chem. B* **2001**, *105*, 604–617.

(8) (a) Strachan, J.-P.; O'Shea, D. F.; Balasubramanian, T.; Lindsey, J. S. *J. Org. Chem.* **2000**, *65*, 3160–3172.(b) Pandey, R. K.; Zheng, G. In *The Porphyrin Handbook*; Kadish, K.M.; Smith, K. M., Guilard, R., Eds.; Academic Press: San Diego, CA, 2000; Vol. 6, pp 157−230. (c) Montforts, F.-P.; Gerlach, B.; Höper, F. *Chem. Rev.* **1994**, *94*, 327–347.(d) Smith, K. M. In *Chlorophylls*; Scheer, H., Ed.; CRC Press: Boca Raton, FL, 1991; pp 115−143. (e) Taniguchi, M.; Ra, D. Y.; Mo, G.; Balasubramanian, T.; Lindsey, J. S. *J. Org. Chem.* **2001**, *66*, 7342–7354.

(9) (a) Hindin, E.; Kirmaier, C.; Diers, J. R.; Tomizaki, K. Y.; Taniguchi, M.; Lindsey, J. S.; Bocian, D. F.; Holten, D. *J. Phys. Chem. B* **2004**, *108*, 8190–8200. (b) Taniguchi, M.; Kim, H. J.; Ra, D. Y.; Schwartz, J. K.; Kirmaier, C.; Hindin, E.; Diers, J. R.; Prathapan, S.; Bocian, D. F.; Holten, D.; Lindsey, J. S. *J. Org. Chem.* **2002**, *67*, 7329–7342. (c) Wiederrecht, G.P .; Svec, W. A.; Niemczyk, M. P.; Wasielewski, M. R. *J. Phys. Chem.* **1995**, *99*, 8918–8926. (d) Wiederrecht, G. P.; Niemczyk, M. P.; Svec, W. A.; Wasielewski, M. R. *J. Am. Chem. Soc.* **1996**, *118*, 81–88.

(10) (a) Ambroise, A.; Kirmaier, C.; Wagner, R. W.; Loewe, R. S.; Bocian, D. F.; Holten, D.; Lindsey, J. S. *J. Org. Chem.* **2002**, *67*, 3811–3826. (b) Loewe, R. S.; Lammi, R. K.; Diers, J. R.; Kirmaier, C.; Bocian, D. F.; Holten, D.; Lindsey, J. S. *J. Mater. Chem.* **2002**, *12*, 1530–1552. (c) Holten, D.; Bocian, D. F.; Lindsey, J. S. *Acc. Chem. Res.* **2002**, *35*, 57–69. (d) Tomizaki, K.; Loewe, R. S.; Kirmaier, C.; Schwartz, J. K.; Retsek, J. L.; Bocian, D. F.; Holten, D.; Lindsey, J. S. *J. Org. Chem.* **2002**, *67*, 6519–6534. (e) Yu, L.; Lindsey, J. S. *J. Org. Chem.* **2001**, *66*, 7402–7419. (f) Li, J.; Ambroise, A.; Yang, S. I.; Diers, J. R.; Seth, J.; Wack, C. R.; Bocian, D. F.; Holten, D.; Lindsey, J. S. *J. Am. Chem. Soc.* **1999**, *121*, 8927–8940. (g) Yang, S. I.; Seth, J.; Balasubramanian, T.; Kim, D.; Lindsey, J. S.; Holten, D.; Bocian, D. F. *J. Am. Chem. Soc.* **1999**, *121*, 4008–4018. (h) Susumu, K.; Therien, M. J. *J. Am. Chem. Soc.* **2002**, *124*, 8550–8552. (i) Shediac, R.; Gray, M. H. B.; Uyeda, H. T.; Johnson, R. C.; Hupp, J. T.; Angiolillo, P. J.; Therien, M. J. *J. Am. Chem. Soc.* **2000**, *122*, 7017–7033. (i) Kumble, R.; Palese, S.; Lin, V. S.-Y.; Therien, M. J.; Hochstrasser, R. M. *J. Am. Chem. Soc.* **1998**, *120*, 11489–11498.

(11) (a) Cho, H. S.; Rhee, H.; Song, J. K.; Min, C.-K.; Takase, M.; Aratani, N.; Cho, S.; Joo, T.; Kim, D. *J. Am. Chem. Soc.* **2003**, *125*, 5849–5860. (b) Mongin, O.; Hoyler, N.; Gossauer, A. *Eur. J. Org. Chem.* **2000**, *7*, 1193–1197. (c) Osuka, A.; Ikeda, M.; Shiratori, H.; Nishimura, Y.; Yamazaki, I. *J. Chem. Soc., Perkin Trans. 2* **1999**, 1019–1025.

(12) (a) Drain, C. M.; Batteas, J. D.; Flynn, G. W.; Milic, T.; Chi, N.; Yablon, D. G.; Sommers, H. *Proc. Natl. Acad. Sci. U.S.A.* **2002**, *99*, 6498–6502. (b) Milic, T. N.; Chi, N; Yablon, D. G.; Flynn, G. W.; Batteas, J. D.; Drain, C. M. *Angew. Chem., Int. Ed.* **2002**, *41*, 2117–2119. (c) Shi, X.; Barkigia, K. M.; Fajer, J.; Drain, C. M. *J. Org. Chem.* **2001**, *66*, 6513–6522. (d) Drain, C. M.; Shi, X; Milic, T.; Nifiatis, F. *Chem. Commun.* **2001**, *15*, 1418–1420. (e) Balaban, T. S.; Eichhofer, A.; Lehn, J.-M. *Eur. J. Org. Chem.* **2000**, *24*, 4047–4057.

(13) (a) Hunter, C. A.; Tregonning, R. *Tetrahedron* **2002**, *58*, 691–697. (b) Imahori, H.; Yamada, K.; Yoshizawa, E.; Hagiwara, K.;

Okada, T.; Sakata, Y. *J. Porphyrins Phthalocyanines* **1997**, *1*, 55–66. (c) Armaroli, N.; Diederich, F.; Echegoyen, L.; Habicher, T.; Flamigni, L.; Marconi, G.; Nierengarten, J.-F. *New J. Chem.* **1999**, 77–83.

(14) (a) Hunter, C. A.; Sanders, J. K. M.; Beddard, G. S.; Evans, S. *J. Chem. Soc., Chem. Comm.* **1989**, 1765–1767. (b) Maiya, B. G.; Bampos, N.; Kumar, A. A.; Feeder, N.; Sanders, J. K. M. *New J. Chem.* **2001**, *25*, 797–800. (c) Mak, C. C.; Bampos, N.; Darling, S. L.; Montalti, M.; Prodi, L.; Sanders, J. K. M. *J. Org. Chem.* **2001**, *66*, 4476–4486.

(15) Belair, J. P.; Ziegler, C. S.; Rajesh, C. S.; Modarelli, D. A. *J. Phys. Chem. A* **2002**, *106*, 6445–6451.

(16) Alemán, E. A.; Rajesh, C. S.; Ziegler, C. S.; Modarelli, D. A. *J. Phys. Chem.* **2006**, *110*, 8605–8612.

(17) (a) Furuta, H.; Ishizuka, T.; Osuka, A.; Dejima, H.; Nakagawa, H.; Ishikawa, Y. *J. Am. Chem. Soc.* **2001**, *123*, 6207–6208. (b) Furuta, H.; Asano, T.; Ogawa, T. *J. Am. Chem. Soc.* **1994**, *116*, 767–8.

(18) Geier, G. R., III; Haynes, D. M.; Lindsey, J. S. *Org. Lett.* **1999**, *1*, 1455–1458.

(19) (a) Maeda, H.; Furuta, H. *Pure Appl. Chem.* **2006**, *78*, 29–44. (b) Harvey, J. D.; Ziegler, C. J. *J. Inorg. Biochem.* **2006**, *100*, 869–880. (c) Chmielewski, P. J.; Latos-Grazynski, L. *Coord. Chem. Rev.* **2005**, *249*, 2510–2533. (d) Srinivasan, A.; Furuta, H. *Acc. Chem. Res.* **2005**, *38*, 10–20.

(20) Vyas, S.; Hadad, C.; Modarelli, D. A. *J. Phys. Chem. A* **2008**, *112*, 6533–6549.

(21) (a) Gouterman, M. *J. Mol. Spectrosc.* **1961**, *6*, 138. (b) Seybold, P. G.; Gouterman, M. *J. Mol. Spectrosc.* **1969**, *31*, 1–13.

(22) Mu, X. H.; Kadish, K. M. *Langmuir* **1990**, *6*, 51–56.

(23) Fajer, J.; Borg, D. C.; Forman, A.; Dolphin, D.; Felton, R. H. *J. Am. Chem. Soc.* **1970**, *92*, 3451–3459.

(24) Fajer, J.; Davis, M. S. In *The Porphyrins*; Dolphin, D., Ed.; Academic Press: New York, 1979; Vol. 4, pp 197−256.

(25) Kaifer, A. E.; Gómez-Kaifer, M. *Supramolecular Electrochemistry*; Wiley-VCH: Weinheim, 1999;, p 18.

(26) Note: Ferrocene undergoes a fast one-electron oxidation to yield the cationic ferrocinium species at very accessible potentials. Its oxidized form is stable in most organic solvents. Therefore, ferrocene can be used as an internal reference (also known as a reference redox couple) for electrochemical experiments performed in low dielectric solvents that do not permit the use of a standard reference electrode.

(27) Becke, A. D. *J. Chem. Phys.* **1993**, *98*, 5648.

(28) Lee, C.; Yang, W.; Parr, R. G. *Phys. Rev. B* **1988**, *37*, 785.

(29) A description of the Gaussian implementation of density functionals can be found in: Johnson, B. G.; Gill, P. M. W. L.; Pople, J. A. *J. Chem. Phys.* **1993**, *98*, 5612.

(30) Scott, A. P.; Radom, L. *J. Phys. Chem.* **1996**, *100*, 16502–16513.

(31) (a) Tomasi, J.; Persico, M. *Chem. Rev.* **1994**, *94*, 2027–2094. (b) Cossi, M.; Barone, V.; Cammi, R.; Tomasi, J. *Chem. Phys. Lett.* **1996**, *255*, 327–335. (c) Barone, V.; Cossi, M.; Tomasi, J. *J. Chem. Phys.* **1997**, *107*, 3210–3221. (d) Cossi, M.; Barone, V. *J. Chem. Phys.* **1998**, *109*, 6246–6254. (e) Barone, V.; Cossi, M.; Tomasi, J. *J. Comput. Chem.* **1998**, *19*, 404–417. (f) Cramer, C. J.; Truhlar, D. G. *Chem. Rev.* **1999**, *99*, 2161–2200.

(32) Frisch, M. J.; Trucks, G. W.; Schlegel, H. B.; Scuseria, G. E.; Robb, M. A.; Cheeseman, J. R.; Montgomery, J. A., Jr.; Vreven, T.; Kudin, K. N.; Burant, J. C.; Millam, J. M.; Iyengar, S. S.; Tomasi, J.; Barone, V.; Mennucci, B.; Cossi, M.; Scalmani, G.; Rega, N.; Petersson, G. A.; Nakatsuji, H.; Hada, M.; Ehara, M.; Toyota, K.; Fukuda, R.; Hasegawa, J.; Ishida, M.; Nakajima, T.; Honda, Y.; Kitao, O.; Nakai, H.; Klene, M.; Li, X.; Knox, J. E.; Hratchian, H. P.; Cross, J. B.; Bakken, V.; Adamo, C.; Jaramillo, J.; Gomperts, R.; Stratmann, R. E.; Yazyev, O.; Austin, A. J.; Cammi, R.; Pomelli, C.; Ochterski, J. W.; Ayala, P. Y.; Morokuma, K.; Voth, G. A.; Salvador, P.; Dannenberg, J. J.; Zakrzewski, V. G.; Dapprich, S.; Daniels, A. D.; Strain, M. C.; Farkas, O.; Malick, D. K.; Rabuck, A. D.; Raghavachari, K.; Foresman, J. B.; Ortiz, J. V.; Cui, Q.; Baboul, A. G.; Clifford, S.; Cioslowski, J.; Stefanov, B. B.; Liu, G.; Liashenko, A.; Piskorz, P.; Komaromi, I.; Martin, R. L.; Fox, D. J.; Keith, T.; Al-Laham, M. A.; Peng, C. Y.; Nanayakkara, A.; Challacombe, M.; Gill, P. M. W.; Johnson, B.; Chen, W.; Wong, M. W.; Gonzalez, C.; Pople, J. A. *Gaussian 03, Revision C.02*; Gaussian, Inc.: Wallingford, CT, 2004.

(33) Weiss, C. In *The Porphyrins*; Dolphin, D., Ed.; Academic Press: New York, 1978; Vol. III, pp 211−223.

(34) Yang, Y.; Lin, Z. G. *J. Appl. Electrochem.* **1995**, *25*, 259–266.

(35) Sullivan, M. G.; Kötz, R.; Haas, O. *J. Electrochem. Soc.* **2000**, *147*, 308–317.

(36) Sullivan, M. G.; Schnyder, B.; Bärtsch, M.; Alliata, D.; Imhof, R.; Kötz, R. *J. Electrochem. Soc.* **2000**, *147*, 2636–2643.

(37) Furuta, H.; Asano, T.; Ogawa, T. *J. Am. Chem. Soc.* **1994**, *116*, 767–768.

(38) (a) Ghosh, A.; Wondimagegn, T.; Nilsen, H. J. *J. Phys. Chem. B* **1998**, *102*, 10459–10467. (b) Zandler, M. E.; D'Souza, F. *J. Mol. Struct. (THEOCHEM)* **1997**, *401*, 301–314. (c) Szterenberg, L.; Latos-Grazynski, L. *Inorg. Chem.* **1997**, *36*, 6287–6291.

(39) Wilford, J. H.; Archer, M. D.; Bolton, J. R.; Ho, T.-F.; Schmidt, J. A.; Weedom, A. C. *J. Phys. Chem.* **1985**, *89*, 5395–5398.

(40) Armaroli, N.; Diederich, F.; Echegoyen, L.; Habicher, T.; Flamigni, L.; Marconi, G.; Nierengarten, J.-F. *New J. Chem.* **1999**, *23*, 77–83.

(41) Oxidation potentials in the range of ∼0.95−1.08 V (H_2TPP) and ∼0.73−0.82 V (ZnTPP) have been found, referenced vs the standard calomel electrode (SCE) with CH_2Cl_2 as the solvent. See, for example, ref 37.

(42) $H_2TPP^{\bullet+}$ has also been shown to undergo a hydrogen transfer to form the dication, see: Sun, H.; Biffinger, J. C.; DiMagno, S. G. *Dalton Trans* **2005**, 3148–3154.

(43) Strauss, S. H.; Thompson, R. G. *J. Inorg. Biochem.* **1986**, *27*, 173–177.

(44) Guilard, R.; Ratti, C.; Tabard, A.; Richard, P.; Dubois, D.; Kadish, K. M. *Inorg. Chem.* **1990**, *29*, 2532–2540.

(45) Lexa, D.; Maillard, P.; Momenteau, M.; Savéant, J. M. *J. Am. Chem. Soc.* **1984**, *106*, 6321–6323.

(46) Connelly, N. G.; Geiger, W. E. *Chem. Rev.* **1996**, *96*, 877–910.

(47) Kadish, K. M.; Cornillon, J. L.; Yao, C.-L.; Malinski, T.; Gritzner, G. *J. Electroanal. Chem.* **1987**, *235*, 189–207.

(48) Kadish, K. M.; Morrison, M. M. *Bioinorg. Chem.* **1977**, *7*, 107–115.

(49) Armaroli, N.; Diederich, F.; Echegoyen, L.; Habicher, T.; Flamigni, L.; Marconi, G.; Nierengarten, J.-F. *New J. Chem.* **1999**, *23*, 77–83.

(50) Inisan, C.; Saillard, J.-Y.; Guilard, R.; Tabard, A.; Le Mest, Y. *New J. Chem.* **1998**, *22*, 823–830.

(51) Peychal-Heiling, G.; Wilson, G. S. *Anal. Chem.* **1971**, *43*, 550–556.

(52) (a) Boesch, S. E.; Grafton, A. K.; Wheeler, R. A. *J. Phys. Chem.* **1996**, *100*, 10083–10087. (b) Raymond, K. S.; Grafton, A. K.; Wheeler, R. A. *J. Phys. Chem. B* **1997**, *101*, 623–631. (c) Kaszynski, P. *J. Phys. Chem. A* **2001**, *105*, 7626–7633. (d) Baik, M.-H.; Schauer, C. K.; Ziegler, T. *J. Am. Chem. Soc.* **2002**, *124*, 11167–11181. (e) Fontanesi, C.; Benassi, R.; Giovanardi, R.; Marcaccio, M.; Paolucci, F.; Roffia, S. *J. Mol. Struct.* **2002**, *612*, 277–286. (f) Namazian, M. *THEOCHEM* **2003**, *273*, 664–665. (g) Benassi, R.; Ferrarini, P.; Fontanesi, C.; Benedetti, L.; Paolucci, F. *J. Electroanal. Chem.* **2004**, *564*, 231–237. (h) Namazian, M.; Almodarresieh, H. A. *THEOCHEM* **2004**, *686*, 97–102. (i) Camurri, G.; Ferrarini, P.; Giovanardi, R.; Benassi, R.; Fontanesi, C. *J. Electroanal. Chem.* **2005**, *585*, 181–190. (j) Dutton, A. S.; Fukuto, J. M.; Houk, K. N. *Inorg. Chem.* **2005**, *44*, 4024–4028. (k) Fu, Y.; Liu, L.; Yu, H.-Z.; Wang, Y.-M.; Guo, Q.-X. *J. Am. Chem. Soc.* **2005**, *127*, 7227–7234. (l) Shamsipur, M.; Alizadeh, K.; Arshadi, S. *THEOCHEM* **2006**, *758*, 71–74. (m) Yu, A.; Liu, Y.; Li, Z.; Cheng, J.-P. *J. Phys. Chem. A* **2007**, *111*, 9978–9987.

(53) Roy, L. E.; Jakubikova, E.; Guthrie, M. G.; Batista, E. R. *J. Phys. Chem. A* **2009**, *113*, 6745–6750.

(54) Chen, H. L.; Pan, Y. H.; Groh, S.; Hagan, T. E.; Ridge, D. P. *J. Am. Chem. Soc.* **1991**, *113*, 2766–2767.

(55) Nakato, Y.; Abe, K.; Tsubomura, H. *Chem. Phys. Lett.* **1976**, *39* (2), 358–60.

(56) Fukuzumi, S.; Ohkubo, K.; Imahori, H.; Shao, J.; Ou, Z.; Zheng, G.; Chen, Y.; Pandey, R. K.; Fujitsuka, M.; Ito, O.; Kadish, K. M. *J. Am. Chem. Soc.* **2001**, *123*, 10676–10683.

(57) (a) Brédas, J. L.; Silbey, R.; Boudreaux, D. S.; Chance, R. R. *J. Am. Chem. Soc.* **1983**, *105*, 6555. (b) L. Micaroni, L.; Nart, F. C.; Hümmelgen, I. A. *J. Solid State Electrochem.* **2002**, *7*, 55–59. (c) Janietza, S.; Bradley, D. D. C.; Grell, M.; Giebeler, C.; Inbasekaran, M.; Woo, E. P. *Appl. Phys. Lett.* **1998**, *73*, 2453–2455.

(58) Conversion to the Fc+/Fc reference electrode is accomplished using the relationship $E_{Fc+/Fc} = E_{Ag/AgCl} + 0.95$ V in DMF and +1.13 V in CH_2Cl_2: Tsierkezos, N. G. *J. Solution Chem.* **2007**, *36*, 289–302.

(59) Paliteiro, C.; Sobral, A. *Electrochim. Acta* **2005**, *50*, 2445–2451.

(60) Gasyna, Z.; Browett, W. R.; Stillman, M. J. *Inorg. Chem.* **1985**, *15*, 2440–2447.

(61) Fajer, J.; Borg, D. C.; Forman, A.; Dolphin, D.; Felton, R. H. *J. Am. Chem. Soc.* **1970**, *92*, 3452–3459.

(62) Closs, G. L.; Closs, L. E. *J. Am. Chem. Soc.* **1963**, *85*, 818–819. The measurements in this study were recorded in THF using Na reduction..

(63) Mack, J.; Stillman, M. J. *J. Porphyrins Phthalocyanines* **2001**, *5*, 67–76.

(64) Fajer, J.; Borg, D. C.; Forman, A.; Dolphin, D.; Felton, R. H. *J. Am. Chem. Soc.* **1973**, 2739–2741.

(65) (a) Gouterman, M.; Wagnière, G.; Synder, L. C. *J. Mol. Spectrosc.* **1963**, *11*, 108–127. (b) Weiss, C.; Kobayashy, H.; Gouterman, M. *J. Mol. Spectrosc.* **1965**, *16*, 415–450. (c) Rimington, C.; Mason, S. F.; Kennard, O. *Spectrochim. Acta* **1958**, *12*, 65–77. (d) Anex, B. G.; Umans, R. S. *J. Am. Chem. Soc.* **1964**, *86*, 5026–5027. (e) Edwards, L. E.; Dolphin, D. H.; Gouterman, M. *J. Mol. Spectrosc.* **1970**, *35*, 90. (f) Edwards, L.; Dolphin, D. H.; Gouterman, M.; Adler, A. D. *J. Mol. Spectrosc.* **1971**, *38*, 16. (g) Kim, B. F.; Bohandy, J. *J. Mol. Spectrosc.* **1978**, *73*, 332.

(66) van Giesbergen, S. J. A.; Rosa, A.; Ricciardi, G.; Baerends, E. J. *J. Chem. Phys.* **1999**, *111*, 2499.

(67) Gwaltney, S. R.; Bartlett, R. J. *J. Chem. Phys.* **1998**, *108*, 6790–6798.

(68) Parusel, A. B. J.; Grimme, St. *J. Porphyrins Phthalocyanines* **2001**, *5*, 225–232.

(69) The slight differences in the absorption band energies are consistent with solvation effects: Alemán, E. A. *PhD. Dissertation*, University of Akron, 2006.

(70) Alemán, E. A. *PhD. Dissertation*, University of Akron, 2006.